DISCRETE AND CONTINUOUS MODELS AND APPLIED COMPUTATIONAL SCIENCE

Volume 27 Number 3 (2019)

Founded in 1993
Founder: PEOPLES' FRIENDSHIP UNIVERSITY OF RUSSIA

DOI: 10.22363/2658-4670-2019-27-3

Edition registered by the Federal Service for Supervision of Communications, Information Technology and Mass Media
Registration Certificate: ПИ № ФС 77-76317, 19.07.2019

ISSN 2658-7149 (online); 2658-4670 (print)
4 issues per year.
Language: English.

Publisher: Peoples' Friendship University of Russia (RUDN University).
Indexed in Ulrich's Periodicals Directory (http://www.ulrichsweb.com), in Russian Science Citation Index (https://elibrary.ru), EBSCOhost (https://www.ebsco.com), CyberLeninka (https://cyberleninka.ru).

Aim and Scope

Discrete and Continuous Models and Applied Computational Science arose in 2019 as a continuation of RUDN Journal of Mathematics, Information Sciences and Physics. RUDN Journal of Mathematics, Information Sciences and Physics arose in 2006 as a merger and continuation of the series "Physics", "Mathematics", "Applied Mathematics and Computer Science", "Applied Mathematics and Computer Mathematics".

Discussed issues affecting modern problems of physics, mathematics, queuing theory, the Teletraffic theory, computer science, software and databases development.

It's an international journal regarding both the editorial board and contributing authors as well as research and topics of publications. Its authors are leading researchers possessing PhD and PhDr degrees, and PhD and MA students from Russia and abroad. Articles are indexed in the Russian and foreign databases. Each paper is reviewed by at least two reviewers, the composition of which includes PhDs, are well known in their circles. Author's part of the magazine includes both young scientists, graduate students and talented students, who publish their works, and famous giants of world science.

The Journal is published in accordance with the policies of COPE (Committee on Publication Ethics). The editors are open to thematic issue initiatives with guest editors. Further information regarding notes for contributors, subscription, and back volumes is available at http://journals.rudn.ru/miph.

E-mail: miphj@rudn.ru, dcm@sci.pfu.edu.ru.

EDITORIAL BOARD

Computer Design: *A. V. Korolkova*

Address of editorial board:
Ordzhonikidze St., 3, Moscow, Russia, 115419
Tel. +7 (495) 955-07-16, e-mail: publishing@rudn.ru
Editorial office:
Tel. +7 (495) 952-02-50, miphj@rudn.ru, dcm@sci.pfu.edu.ru
site: http://journals.rudn.ru/miph

Paper size 70×1 00/16. Offset paper. Offset printing. Typeface "Computer Modern".
Conventional printed sheet 5,48. Printing run 500 copies. Open price. The order 1091.
PEOPLES' FRIENDSHIP UNIVERSITY OF RUSSIA
6 Miklukho-Maklaya St., 117198 Moscow, Russia
Printed at RUDN Publishing House:
3 Ordzhonikidze St., 115419 Moscow, Russia,
Ph. +7 (495) 952-04-41; e-mail: publishing@rudn.ru

Discrete & Continuous Models
& Applied Computational Science
2019, 27 (3) 204
http://journals.rudn.ru/miph

Contents

Mathematical modeling

Computational modeling and simulation

Discrete & Continuous Models
& Applied Computational Science
2019, 27 (3) 205–216
http://journals.rudn.ru/miph

Mathematical modeling

Research article

UDC 51-73 519.6 519.8
PACS 07.05.Tp, 02.60.Pn, 02.70.Bf
DOI: 10.22363/2658-4670-2019-27-3-205-216

Simulation of a gas-condensate mixture passing through a porous medium in depletion mode

Alina V. Volokhova[1], **Elena V. Zemlyanaya**[1,2], **Vladimir V. Kachalov**[3], **Victor S. Rikhvitsky**[1], **Vadim N. Sokotushchenko**[2,3]

[1] *Joint Institute for Nuclear Research*
6 Joliot-Curie St., Dubna, Moscow Region 141980, Russian Federation
[2] *State University "Dubna"*
19 Universitetskaya St., Dubna, Moscow Region 141980, Russian Federation
[3] *Joint Institute for High Temperatures of Russian Academy of Sciences*
13 Bd.2 Izhorskaya St., Moscow 125412, Russian Federation

(received: December 6, 2019; accepted: December 23, 2019)

One of important tasks in a development of gas-condensate fields is to minimize hydrocarbons loss arising from the gas condensation in pores of the gas-bearing layer. The search for the optimal gas production regime is carried out both on the basis of laboratory experiments and on the base of computer simulation. In this regard, the relevant is the verification of the constructed mathematical models by means of comparison of numerical results with experimental data obtained on the laboratory models of a hydrocarbon reservoirs. Within the classical approach on the basis of the Darcy law and the law continuity for flows, the model is formulated that describes the passing a multicomponent gas-condensate mixture through a porous medium in the depletion mode. The numerical solution of the corresponding system of nonlinear partial differential equations is implemented on the basis of the combined use of the C++ programming language and the Maple software. Shown that the approach used provides an agreement of results of numerical simulations with experimental data on the dynamics of hydrocarbon recoverability depending on the pressure obtained at VNIIGAZ, Ukhta.

Key words and phrases: computer simulations, multicomponent hydrocarbon system, nonlinear partial differential equations, finite difference approximation, passing of gaz-condensate mixture through a porous medium

1. Introduction

Recently, due to the decrease in easily recoverable natural gas reserves in traditional fields, the development of areas with unconventional hydrocarbon reserves, including gas-condensate fields, has attracted attention [1]–[3]. Gas production in such fields is difficult due to the presence of the condensate [4]–[6]. Methods for increasing the gas production based on reducing a condensation is reviewed in the recent paper [7]. The behavior of a multi-component gas-condensate mixture in a porous medium can be difficult to predict. Indeed, the phase states of the components can change. Gas has a much lower viscosity than liquid, thus a boiling of any component gives it an advantage in the speed of passage. The movement of the mixture is caused by the pressure drop at the point of its extraction. The pressure drop leads, in turn, to the possibility of boiling, that is, the phase transition of any component from a liquid to a gaseous state. A paradoxical result may be the formation of a condensate plug if the gas thus "erode".

In this regard, the development of realistic mathematical models can help predict the physical and technological parameters that ensure optimization of the gas production regime in the gas-condensate reservoirs. One of actual problems in this direction is the verification of mathematical models developed on the basis of the comparison of numerical results with the data of practical measurements, including the data of laboratory experiments. Traditionally, an approach based on the classical Darcy law and conservation laws, described in detail in the literature, is used to model the processes of passage of multicomponent gas-condensate mixtures through a porous medium (see, for example, [8]–[13] and references therein). In this framework, one formulates the system of equations with appropriate initial and boundary conditions tailored to the specific modeling process, including the geometry of the system, physical-chemical parameters of the studied process and other factors. In [14], basing on the numerical solution of a stationary system of equations we obtained an agreement of numerical results with experimental data from [15] on stabilization of a two-component gas-condensate mixture passing through a porous medium. In [16], the experimental results of [17] on the dynamics of extraction of heavy components of a multicomponent hydrocarbon mixture in the depletion mode are numerically reproduced in the assumption of a homogeneous spatial distribution of the pressure and the density of hydrocarbons.

This work is a continuation of our studies on the numerical analysis of measurements at VNIIGAZ, Ukhta [17]. As previously, our consideration is based on the mathematical model described by the Darcy law and the law of continuity of flows. The approach developed in [16] is generalized to the case of taking into account the coordinate dependence of physical characteristics of the system modeled. Based on a numerical solution of the formulated initial-boundary value problem for a system of nonlinear partial differential equations, an adequate agreement is obtained between the numerical results and the experimental data from [17] on the yield of both heavy and light hydrocarbons in the laboratory model of the gas-bearing formation at a temperature of 25°C. In the paper, the mathematical formulation of the problem is given, the computational scheme implemented as a package of C++ and Maple programs is described, and the results of computer simulations are presented.

2. General statement of the problem

In general, the dynamic process of the passing the n-component gas-condensate mixture of hydrocarbons through a porous medium is described by a system of equations

$$u_\alpha = -\frac{k_\alpha}{\mu_\alpha}\nabla P_\alpha, \tag{1}$$

$$\frac{\partial \rho_{i\,\alpha}}{\partial t} + \nabla(u_\alpha \rho_{i\,\alpha}) = V_{i\,\alpha}. \tag{2}$$

Here, the first equation (1) corresponds to the Darcy law, and the the second one (2) — to the flows continuity law, $V_{i\alpha}$ – interfacial transition rates.

The process involves n components: $i = 1 \dots n$, located at pressure P_α in the α-phase, where $\alpha = L$ corresponds to the liquid phase, and $\alpha = G$ to the gaseous phase.

For components in the α phase, the u_α is the linear flow velocity, k_α and μ_α are, respectively, the parameters of permeability and viscosity of the α-phase, $\rho_{i\,\alpha}$ is the molar density of the i-th component in α-phase (defined as the local volume average).

It is assumed that the gas and liquid in the pores occupy a separate volumes divided by the interfacial surface, on which there are surface tension forces. Concentrations of components in gas and liquids are different, depending on time and coordinate. Inside the gas and liquid, the pressure P is described by the Peng-Robins equation:

$$P_\alpha = P_\alpha(v_\alpha) = \frac{RT}{v_\alpha - b_{m\alpha}} - \frac{a_{m\alpha}}{v_\alpha(v_\alpha + b_{m\alpha}) + b_{m\alpha}(v_\alpha - b_{m\alpha})}. \tag{3}$$

Here R is the gas constant, T is the temperature, v_α is the molar volume taking into account for a porosity m and the gas saturation S_α

$$v_\alpha = \frac{mS_\alpha}{\rho_\alpha}, \quad \rho_\alpha = \sum_{i=1}^{n} \rho_{i\,\alpha}. \tag{4}$$

The constants $a_{m\alpha}$ and $b_{m\alpha}$ are defined as follows [18], [19]:

$$a_{m\alpha} = \frac{R^2T^2}{P_\alpha}A_{m\alpha}, \quad b_{m\alpha} = \frac{RT}{P_\alpha}B_{m\alpha},$$

$$A_{m\alpha} = \sum_{i,j=1}^{n}(1-k_{ij})(A_{i\,\alpha}A_{j\,\alpha})^{1/2}C_{i\,\alpha}C_{j\,\alpha}, \quad B_{m\alpha} = \sum_{i=1}^{n} B_{i\,\alpha}C_{i\,\alpha},$$

$$A_{i\,\alpha} = 0.4572355\frac{P^r_{i\,\alpha}}{T^r_i}\left[(0.37464 + 1.5422\omega_i - 0.02699\omega_i^2)(1-(T^r_i)^{1/2}) + 1\right]^2,$$

$$B_{i\,\alpha} = 0.077796074P^r_{i\,\alpha}/T^r_i, \quad P^r_{i\,\alpha} = P_{i\,\alpha}/P_i^{crit}, \quad T^r_i = T/T_i^{crit}.$$

Here ω_i is the acentric factor of the i-th component, P_i^{crit} and T_i^{crit} are the critical pressure and the temperature.

The gas saturation S_G is defined as the maximal root of the equation

$$P_G = P_G\left(\frac{mS_G}{\rho_G}\right) = P_L\left(\frac{m(1-S_G)}{\rho_L}\right) + P_{\text{capillar}}, \quad S_G + S_L = 1, \quad 0 \leqslant S_\alpha \leqslant 1. \tag{5}$$

The molar fractions of the components in the liquid and gas phases $C_{i\alpha}$ in the formulas for $A_{i\alpha}$ and $B_{i\alpha}$ are calculated as

$$C_{i\,\alpha} = \frac{\rho_{i\,\alpha}}{\rho_\alpha}. \tag{6}$$

Interfacial transition rates satisfy the condition

$$V_{i\,G} + V_{i\,L} = 0 \tag{7}$$

and are determined from the following relation:

$$V_{i\,\alpha} = \eta_i(\phi_i^{\bar{\alpha}} - \phi_i^\alpha), \quad \text{where} \quad \bar{G} = L,\ \bar{L} = G, \tag{8}$$

where ϕ_i^L, ϕ_i^G are the Gibbs chemical potentials of the i-th component, η_i is the interfacial coefficient transition, depending on many factors, including the structure of the rock.

Potential formulae are derived in [19] from equation (3):

$$\frac{\phi_i^\alpha}{RT} = \ln(P_\alpha C_{i\,\alpha}) + \frac{B_{i\,\alpha}}{B_{m\alpha}}(Z_\alpha - 1) - \ln(Z_\alpha - B_{m\alpha}) + \\ + \frac{A}{\sqrt{2}B_{m\alpha}}\left(\frac{\sum\limits_{j=1}^{n}(1-k_{ij})(A_{i\,\alpha}A_{j\,\alpha})^{1/2}C_{j\,\alpha}}{A_{m\alpha}} - \frac{B_{i\,\alpha}}{2B_{m\alpha}}\right) \times \\ \times \ln\left(\frac{Z_\alpha + (1-\sqrt{2})B_{m\alpha}}{Z_\alpha + (1+\sqrt{2})B_{m\alpha}}\right), \tag{9}$$

where

$$Z_\alpha = \frac{P_\alpha v_\alpha}{RT}. \tag{10}$$

Note that in case $P_{\text{capillar}} = 0$, taking into account for (10), the gas saturation S_G can be calculated from the equation

$$\frac{Z_L}{Z_G} = \frac{\rho_G(1-S_G)}{\rho_L S_G}. \tag{11}$$

Here Z_α are the roots of the equation (following from (3))

$$f_\alpha(Z) = Z^3 + (B_{m\alpha} - 1)Z^2 + (A_{m\alpha} - 3B_{m\alpha}^2 - 2B_{m\alpha})Z + \\ + B_{m\alpha}(-A_{m\alpha} + B_{m\alpha}^2 + B_{m\alpha}) = 0, \tag{12}$$

such that

$$Z_G = \max\{Z : f_G(Z) = 0\}, \quad Z_L = \min\{Z : f_L(Z) = 0\}. \tag{13}$$

In the experiment [17], where a gas-condensate mixture passes through a long pipe filled with a porous substance, it is natural to consider the spatially one-dimensional case with a single coordinate along the pipe. In this case, the differentiation operator will have the form $\nabla f = \dfrac{\partial}{\partial x} f$. Note that the problem has a simple generalization to the case of a thin gas-bearing formation with circular symmetry. In this case, when passing to the polar coordinate system, the differentiation operator takes the form $\nabla f = \dfrac{1}{r}\dfrac{\partial}{\partial r}(rf)$.

3. Laboratory experiment

In the experiment [17], the laboratory model (LM) of the gas-bearing formation is a thermostatic cylinder with a narrow pipe (core holder) of 3 cm in diameter and 93.27 cm long inside. A pipe filled with a terrigenous filler with porosity of $m = 0.1377$, has been saturating under the pressure of 35 MPa with a nine-component hydrocarbon mixture of CH_4, C_3H_8, nC_4H_{10}, nC_6H_{14}, nC_7H_{16}, nC_9H_{20}, $nC_{10}H_{22}$, $nC_{12}H_{26}$, $nC_{16}H_{34}$ in molar concentrations, respectively, of 87.01%; 7.00%; 1.11%; 0.70%; 0.86%; 1.19%; 0.94%; 1.02%; 0.17%, and both ends of the pipe are closed. After the achievement of the phase equilibrium in LM, one end of the tube is opened that provides a gradual release of the substance through this end while maintaining a constant rate of its consumption by means of a regulating the pressure reduction not more than 0.2 MPa/h. The yield of heavy (C_{5+}) and light (C_{2-4}) hydrocarbons in both liquid and gas phases depending on the pressure were measured. Aggregate C_{5+} includes components nC_6H_{14}, nC_7H_{16}, nC_9H_{20}, $nC_{10}H_{22}$, $nC_{12}H_{26}$, $nC_{16}H_{34}$ of the hydrocarbon mixture, and the aggregate C_{2-4} consists of components CH_4, C_3H_8, nC_4H_{10}. The experiment was carried out at two temperature values: $T = 25^\circ$C and $T = 60^\circ$C. Here, we present numerical results only in case $T = 25^\circ$C.

4. Computational scheme and implementation

Taking into account the conditions the laboratory experiment, we consider here a spatially one-dimensional case. Since the time t and the coordinate x do not enter explicitly into the system (1), (2), we pass to arbitrary units, assuming, in particular, $x \in [0, 1]$. The end of $x = 1$ is always closed; the mixture is extracted through the point $x = 0$.

To numerically solve the system of equations (1), (2), a discrete mesh in coordinate is introduced with the step $h_x = 1/N$, with main nodes $x_k = h_x/2 + (k-1) \cdot h_x$ and intermediate nodes $x_{k\pm1/2} = x_k \pm h_x/2$, where $k = 1, \ldots, N$, N is a number of the discrete mesh nodes.

The difference equations at the nodes x_k take the form:

$$u_\alpha^{(k-1/2)} = -\frac{k_\alpha}{\mu_\alpha}\,\frac{P_\alpha^{(k-1)} - P_\alpha^{(k)}}{x_{k-1} - x_k}, \tag{14a}$$

$$\frac{\partial \rho_{i\,\alpha}^{(k)}}{\partial t} + \frac{u_\alpha^{(k+1/2)}\rho_{i\,\alpha}^{(k+1/2)} - u_\alpha^{(k-1/2)}\rho_{i\,\alpha}^{(k-1/2)}}{x_{k+1/2} - x_{k-1/2}} = V_{i\,\alpha}^{(k)}, \tag{14b}$$

$$\rho_{i\,\alpha}^{(k-1/2)} = \frac{1}{2}\Big(\rho_{i\,\alpha}^{(k)} + \rho_{i\,\alpha}^{(k-1)}\Big) - \frac{1}{8}\Big(\rho_{i\,\alpha}^{(k-1)} - 2\rho_{i\,\alpha}^{(k)} + \rho_{i\,\alpha}^{(k+1)}\Big). \tag{14c}$$

Here $u_\alpha^{(k)} = u(t, x_k)_\alpha$, $\rho_{i\alpha}^{(k)} = \rho(t, x_k)_{i\alpha}$, k is the number of a coordinate node.

The difference equations (14) can be interpreted as the modeling the original (one-dimensional) object as a set of cells $x \in [x_{k-1/2}, x_{k+1/2}]$, where $\rho_{i\,\alpha}^{(k)}$, $P_\alpha^{(k)}$ and $S_\alpha^{(k)}$ are, respectively, the average density of i-component, the pressure and the saturation of the α-phase inside each cell. Values $\rho_{i\,\alpha}^{(k\pm1/2)}$ and $u_\alpha^{(k\pm1/2)}$ are, respectively, the density of i-components at the boundaries between cells and the linear velocity of the i-components across the boundaries.

Note that the scheme (14) allows a simple generalization on the spatially two-dimensional case for a plane gas-bearing layer with circular symmetry.

The boundary condition for u_α at the closed end $x = 1$ has the form $u_\alpha|_{x=1} = 0$ or, in terms of the difference scheme, $u_\alpha^{(N+1/2)} = 0$. As for the end $x = 0$, it is also closed until $t = 0$, i.e. $u_\alpha|_{x=0,t\leqslant 0} = 0$ or $u_\alpha^{(1/2)} = 0$. For $t > 0$, taking into account the phase equilibrium achieved under the experimental conditions and the constant yield of the hydrocarbon substance, the boundary condition is formulated as $(u_\alpha\rho_\alpha)|_{x=0} = q_\alpha|_{x=0}$, where $q_\alpha|_{x=0}$ is the given constant. The initial conditions for the functions $\rho_{i\alpha}$ are chosen so that the pressure at the initial time is equal to 35 MPa.

To the numerical solution of the Cauchy problem for the system (14), the fourth-order Runge–Kutta method is implemented as a combined Maple/C++ code, where The Maple part is responsible for the input data, saving and visualization of the results, while the numerical solution of the system (14) is written in C++, which, as practice has shown, provides a faster calculation compared to the previously developed pure Maple implementation.

As in the previous work [16], the numerical simulation continued until the pressure as a result of MP depletion was reduced to 1 atm. The calculations were performed with the coordinate step $h_x = 0.1$ and the time step of 0.0001. The values of the parameters determining the physicochemical properties of components in the hydrocarbon mixture are taken from [20]. In calculations we assumed $P_G = P_L$.

The interphase transition coefficient η_i was chosen in the form $\eta_i = \eta_0 M_i^\varkappa m$, where M_i is the molar weight of i-th component, η_0 and $\varkappa$ are constants to be varied in order to adequately reproduce the experimental data. The ratios of viscosity to permeability parameters in the L and G phases in equation (1) ($\lambda_L = \frac{k_L}{\mu_L}$ and $\lambda_G = \frac{k_G}{\mu_G}$) were also adjusted to the experimental data.

The best agreement with the set of experimental data from [17] for the case $T = 25^{\circ}C$ was obtained at $\eta_0 = 0.001713$, $\varkappa = 1.370349$, $\lambda_L = 0.004631 \times 10^{-7}$, $\lambda_G = 2.073255 \cdot 10^{-7}$.

5. Results of computer simulations

Figure 1(a) and Figure 1(b) show the pressure dynamics P and gas saturation S_G at the points $x = 0.05$, $x = 0.45$, and $x = 0.85$ which are, respectively, near the exit from the LM (solid curves), in the central part of the LM (dashed), and near the closed end (dotted). As in the laboratory experiment, the calculated P decreases during the LM depletion. It can be seen that P in different parts of the LM is different: closer to the exit region of LM, P is less and faster tends to zero.

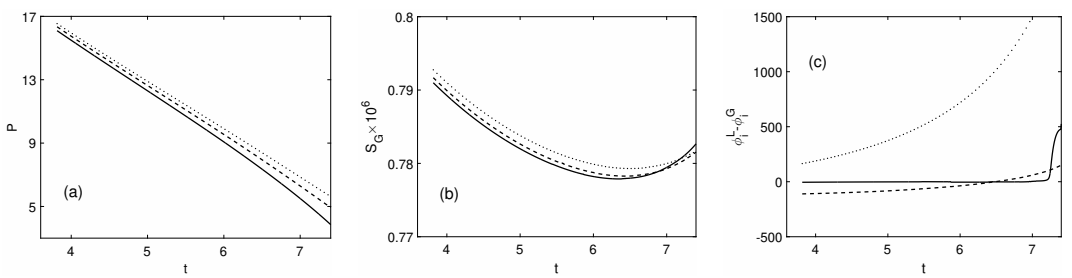

Figure 1. Evolution of the pressure $P = P_G = P_L$ in MPa (a) and of the gas saturation S_G (b) in the region of exit from the LM (solid curve), in the central region of the LM (dashed curve) and in the closed end region (dotted curve).
(c) Evolution of the chemical potential difference (J/mol) for the components nC_9H_{20} (solid), C_3H_8 (dashed) and CH_4 (dotted) at the point $x = 0.05$ in the exit region of the LM

The saturation values in different regions of the LM also differ. When P drops in process of depletion, the saturation slightly decreases, and at the final of the depletion process, at low P, it noticeably increases in the region of the LM exit.

The phase equilibrium reached according to the experimental conditions by the time $t = 0$, begins to be disturbed when the transport factor is turned on, especially at the of the depletion process. This is confirmed by the increase in the chemical potential difference (J/mol) shown in Figure 1(c) for the components nC_9H_{20} (solid), C_3H_8 (dashed) and CH_4 (dotted) at the point $x = 0.05$ corresponding to the exit region of LM.

Figure 2 shows the evolution of the molar densities of the gas components $nC_{16}H_{26}$ (dash-dotted line), $nC_{10}H_{22}$ (solid), nC_9H_{20} (dashed), nC_6H_{14} (dotted line) at the points $x = 0.05$, $x = 0.35$, and $x = 0.85$ which correspond to the exit region from LM (Figure 2(a)), the internal region of LM (Figure 2(b)) and the closed end region (Figure 2(c)). During the depletion process, the density of each hydrocarbon component decreases. The "bursts" of increasing concentrations in the graphs can be explained by the transition of hydrocarbon components from the condensed phase to the gaseous state (boiling) due

to the pressure drop. It can be seen that the boiling begins with the heaviest hydrocarbons and is observed first in the exit region of LM (Figure 2(a)), where the pressure is the lowest. This effect requires the further studies.

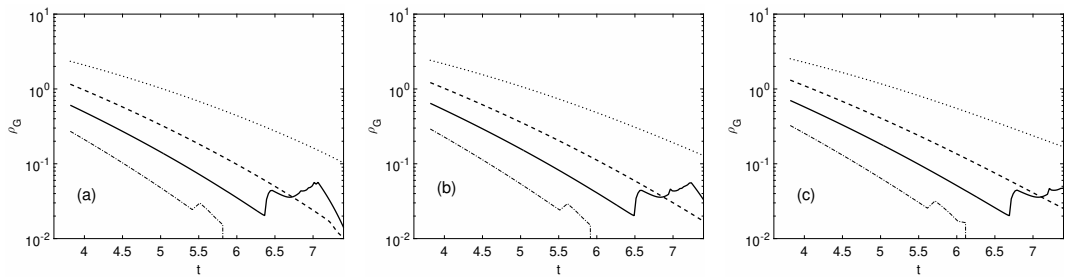

Figure 2. Evolution of molar densities of gas components $nC_{16}H_{26}$ (dash-dotted line), $nC_{10}H_{22}$ (solid), nC_9H_{20} (dashed), nC_6H_{14} (dotted line) in the exit region of the LM (a), in the inner region of the LM (b) and in the closed end region (c)

Figure 3 shows the results of calculating the yields of heavy (C_{5+}) and light (C_{2-4}) hydrocarbons depending on the pressure in comparison with experimental data from [17] at temperature 25°C. It is seen that the developed approach provides adequate reproduction of the laboratory experiments. In particular, computer simulation confirms some increase in the recoverability of hydrocarbons at low pressure, which occurs, as can be seen from Figure 2, due to the transition of part of the condensate into a gaseous state.

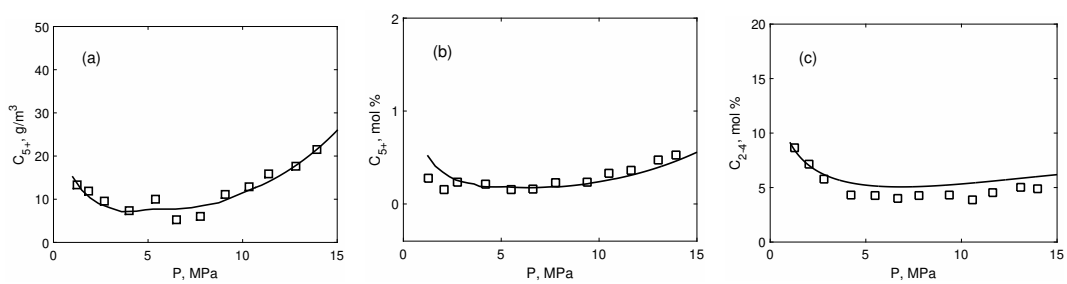

Figure 3. (a) Dependence of the yield (g/m3) of heavy hydrocarbons C_{5+} on the pressure at the outlet of the MP in the depletion mode at a temperature of 25^{o}C in comparison with the experimental data from [17].
(b) Dependence of the molar fraction (in %) of heavy hydrocarbons C_{5+} on the pressure at the outlet of the MP in the depletion mode at a temperature of 25^{o}C in comparison with the experimental data from [17].
(c) Dependence of the molar fraction (in %) of light hydrocarbons C_{2-4} on the pressure at the outlet of the MP in the depletion mode at a temperature of 25°C in comparison with the experimental data from [17]

6. Conclusions

The mathematical formulation of the problem and the Maple/C++ implementation has been developed for numerical simulation of the process of

extraction of multi-component hydrocarbon gas-condensate composition in the depletion mode. Accounting for the hydrocarbons distribution along the length of the LM allowed one to well reproduce the experimental data on the yield of heavy and light hydrocarbons as a function of pressure obtained at laboratory model of the reservoir at the temperature of 25°C (VNIIGAZ, Ukhta) [17]. Currently, similar calculations are carried out to analyze experimental data obtained at the temperature of 60°C. In conclusion, we note that the calculations presented were carried out with a relatively small number of nodes of a discrete mesh at x. Increasing the calculation accuracy, as well as modeling two-dimensional systems based on the proposed difference scheme, requires a significant increase in computer time, which makes the parallel implementation of the presented computational scheme using parallel programming technique relevant.

Acknowledgments

This work was supported by the Russian Foundation for Basic Research (Grant No. 17-08-01270A).

References

[1] Z. P. Sklyarova, F. S. Sokolov, and V. S. Tkach, "Characteristics of the raw materials base of condensate [Kharakteristika syr'yevoy bazy kondensata]," *Groups Gazprom. Conduct a gas science*, vol. 18, no. 2, pp. 4–14, 2014, in Russian.

[2] R. I. Vyakhirev, A. I. Gritsenko, and R. M. Ter-Sarkisov, *Development and operation of gas fields [Razrabotka i ekspluatatsiya gazovykh mestorozhdeniy]*. Moscow: Nedra, 2002, 880 pp., in Russian.

[3] V. M. Zaichenko, I. L. Maikov, and V. M. Torchinskii, "Features of hydrocarbon mixtures filtration in a porous medium," *High Temperature*, vol. 51, no. 6, pp. 776–784, 2013. DOI: 10.1134/S0018151X13050222.

[4] V. M. Zaichenko, I. L. Maikov, V. M. Torchinskii, and E. E. Shpil'rain, "Simulation of processes of filtration of hydrocarbons in a gas-condensate stratum," *High Temperature*, vol. 47, pp. 669–674, 5 2009. DOI: 10.1134/S0018151X09050083.

[5] O. A. Lobanova and I. M. Indrupsky, "Modeling the mutual influence of hydro- and thermodynamics processes in the filtration of hydrocarbon systems [Modelirovaniye vzaimovliyaniya gidro- i termodinamicheskikh protsessov pri fil'tratsii uglevodorodnykh sistem]," *Automation, telemechanization and communication in the oil industry*, pp. 19–23, 10 2010, in Russian.

[6] O. A. Lobanova and I. M. Indrupsky, "Nonequilibrium of the phase behavior of hydrocarbon systems: modeling and scale effect [Neravnovesnost' fazovogo povedeniya uglevodorodnykh sistem: modelirovaniye i masshtabnyy effekt]," in *Abstracts of the IX All-Russian scientific and technical conference "Actual problems of development of the Russian oil and gas complex"*, in Russian, 2012, pp. 96–97.

[7] A. V. Volokhova, E. V. Zemlyanaya, V. V. Kachalov, and V. N. Sokotushchenko, "Overview of the component enhancement methods in development of the gas condensate fields [Obzor metodov povysheniya komponentootdachi pri razrabotkakh gazokondensatnykh mestorozhdeniy]," *The science. Innovations. Technologies*, vol. 3, pp. 19–48, 2019, in Russian.

[8] K. Aziz and A. Settary, *Petroleum reservoir simulation*. London: Applied Science Publishers Ltd, 1979, 476 pp.

[9] I. N. Ponomareva and V. A. Mordvinov, *Underground hydromechanics [Podzemnaya gidromekhanika]*. Perm: Perm state technical university, 2009, 103 pp., in Russian.

[10] V. S. Mitlin, *Underground hydromechanics of complex hydrocarbon mixtures [Podzemnaya gidromekhanika slozhnykh uglevodorodnykh smesey]*. Moscow: VINITI, 1991, vol. 4, 154–222, in Russian.

[11] G. T. Bulgakova, T. A. Faizullin, and A. V. Zhiber, "Nonequilibrium two-phase filtration [Neravnovesnaya dvukhfaznaya fil'tratsiya]," *Matematicheskoye modelirovaniye*, vol. 18, no. 10, pp. 19–38, 2006, in Russian.

[12] D. O. Dil and A. M. Bubenchikov, "Diphasic filtration in a pipe filled with porous material [Dvukhfaznaya fil'tratsiya v trube, zapolnennoy poristym materialom]," *Bulletin of Tomsk State University*, Mathematics and Mechanics, vol. 5 (25), pp. 45–51, 2013, in Russian.

[13] A. L. Kovalev and Y. V. Sheberstov, "Numerical simulation of non-equilibrium local filtration in gas-condensate beds [Chislennoye modelirovaniye lokal'no-neravnovesnoy fil'tratsii v gazokondensatnykh plastakh]," *News of gas science*, no. 5 (37), pp. 164–171, 2018, in Russian.

[14] A. V. Volokhova, E. V. Zemlyanaya, V. V. Kachalov, V. N. Sokotushchenko, and V. S. Rikhvitskiy, "Numerical investigation of the gas-condensate mixture flow in a porous medium [Chislennoye issledovaniye fil'tratsii gazokondensatnoy smesi v poristoy srede]," *Computer Research and Modeling*, vol. 10, no. 2, pp. 209–219, 2018, in Russian.

[15] H. X. Vo, "Composition Variation During Flow of Gas-Condensate Wells," Department of energy resources engineering of Stanford University, Tech. Rep., 2010.

[16] A. V. Volokhova, E. V. Zemlyanaya, V. V. Kachalov, V. S. Rikhvitsky, and V. N. Sokotustchenko, "Numerical modeling of dynamics of extraction of multicomponent gas-condensate hydrocarbon mixture in the mode of depletion of the filtration model of the formation [Chislennoye modelirovaniye dinamiki izvlecheniya mnogokomponentnoy gazokondensatnoy uglevodorodnoy smesi v rezhime istoshcheniya fil'tratsionnoy modeli plasta]," *Geoinformatika*, vol. 3, pp. 27–33, 2019, in Russian.

[17] A. N. Volkov, V. L. Lapshin, and A. V. Polyakov, "Simulation of gaz condensate system phase beghavior in porous media [Modelirovaniye fazovogo povedeniya gazokondensatnoy sistemy v poristoy srede]," *Gaz Industry Magazine*, no. 10, pp. 26–31, 2016, in Russian.

[18] V. G. Lysov and Y. G. Rykov, "On calculation of phase equilibrium in multicomponent filtration problems [O vychislenii fazovogo ravnovesiya v zadachakh mnogokomponentnoy fil'tratsii]," *IPM Preprint im. M. V. Keldysh Russian Academy of Sciences*, no. 94, 2014, in Russian.

[19] A. I. Brusilovsky, *Phase transformations in the development of oil and gas fieldse [Fazovyye prevrashcheniya pri razrabotke mestorozhdeniy nefti i gaza]*. Grail, 2002, 575 pp., in Russian.

[20] L. B. Director, V. V. Kachalov, I. L. Maikov, and S. N. Skovorodko, *One-dimensional nonstationary model of two-phase filtration of a gas-condensate mixture [Odnomernaya nestatsionarnaya model' dvukhfaznoy fil'tratsii gazokondensatnoy smesi]*, 2–xs441. 2000, 45 pp., in Russian.

For citation:

A. V. Volokhova, E. V. Zemlyanaya, V. V. Kachalov, V. S. Rikhvitsky, V. N. Sokotushchenko, Simulation of a gas-condensate mixture passing through a porous medium in depletion mode, Discrete and Continuous Models and Applied Computational Science 27 (3) (2019) 205–216. DOI: 10.22363/2658-4670-2019-27-3-205-216.

Information about the authors:

Alina V. Volokhova — Junior Researcher of Joint Inststute of Nuclear Research (e-mail: `bskr@yandex.ru`, phone: +7(49621)63959, ORCID: https://orcid.org/0000-0002-8122-7340, Scopus Author ID: 56505574900)

Elena V. Zemlyanaya — Doctor of Physical and Mathematical Sciences, Head of sector of Joint Inststute of Nuclear Research, Professor of State University "Dubna" (e-mail: `elena@jinr.ru`, phone: +7(49621)64728, ORCID: https://orcid.org/0000-0001-8149-9533, ResearcherID: B-8160-2016, Scopus Author ID: 6701729810)

Vladimir V. Kachalov — Candidate of Technical Sciences, Senior Researcher of Joint Institute for High Temperatures of Russian Academy of Sciences (e-mail: `ongk@mail.ru`, phone: +7(495)4859145, ORCID: https://orcid.org/0000-0002-6642-4899, Scopus Author ID: 6701510830)

Victor S. Rikhvitsky — Leading Programmer of Joint Inststute of Nuclear Research (e-mail: `rqvtsk@mail.ru`, phone: +7(49621)63811, ORCID: https://orcid.org/0000-0001-6597-7443, Scopus Author ID: 57190934347)

Vadim N. Sokotushchenko — Candidate of Technical Sciences, Associate Professor of State University of Dubna, Leading Engineer of Joint Institute for High Temperatures of Russian Academy of Sciences (e-mail: `sokotushenko@mail.ru`, phone: +7(962)9515352, ORCID: https://orcid.org/0000-0002-9665-269X, Scopus Author ID: 57192655832)

УДК 51-73 519.6 519.8
PACS 07.05.Tp, 02.60.Pn, 02.70.Bf
DOI: 10.22363/2658-4670-2019-27-3-205-216

Моделирование прохождения газоконденсатной смеси через пористую среду в режиме истощения

А. В. Волохова[1], **Е. В. Земляная**[1,2], **В. В. Качалов**[3], **В. С. Рихвицкий**[1], **В. Н. Сокотущенко**[2,3]

[1] *Объединённый институт ядерных исследований*
ул. Жолио Кюри, д. 6, г. Дубна, Московская область, 141980, Россия
[2] *Государственный университет «Дубна»*
ул. Университетская, д. 19, г. Дубна, Московская область, 141980, Россия
[3] *Объединённый институт высоких температур РАН*
ул. Ижорская, д. 13, стр. 2, г. Москва, 125412, Россия

Одной из важных задач при разработке газоконденсатных месторождений является минимизация потерь извлекаемых углеводородов, возникающих из-за конденсации газа в порах пласта. Поиск оптимальных режимов газодобычи производится как на основе лабораторных экспериментов, так и на основе компьютерного моделирования. В этой связи актуальность приобретает верификация построенных математических моделей на основе сопоставления расчётных данных с данными, полученными в ходе экспериментов на лабораторной модели пласта. В рамках классического подхода, основанного на законе Дарси и законе неразрывности потоков, сформулирована модель, описывающая прохождение многокомпонентной газоконденсатной смеси через пористую среду в режиме истощения. Численное решение соответствующей системы нелинейных уравнений в частных производных реализовано на основе комбинированного применения C++ и Maple. Показано, что используемый подход обеспечивает количественное согласие полученных численных результатов с экспериментальными данными, полученными в ВНИИГАЗ (г. Ухта), по динамике извлекаемости углеводородов в зависимости от давления.

Ключевые слова: компьютерное моделирование, многокомпонентная система углеводородов, нелинейные дифференциальные уравнения в частных производных, конечно-разностная аппроксимация, прохождение газоконденсатной смеси через пористую среду

Research article

UDC 519.6
DOI: 10.22363/2658-4670-2019-27-3-217-230

Charge diffusion in homogeneous molecular chains based on the analysis of generalized frequency spectra in the framework of the Holstein model

Dmitry A. Tikhonov[1,2], Egor V. Sobolev[1,3], Victor D. Lakhno[1]

[1] *Institute of Mathematical Problems of Biology*
Branch of Keldysh Institute of Applied Mathematics of RAS
1 Professor Vitkevich St., Pushchino, Moscow Region 142290, Russian Federation
[2] *Institute of Theoretical and Experimental Biophysics of RAS*
3 Institutskaya St., Pushchino, Moscow Region 142290, Russian Federation
[3] *European Molecular Biology Laboratory, Hamburg Unit*
c/o DESY, Building 25A, Notkestraße 85, 22607 Hamburg, Germany

(received: November 12, 2019; accepted: December 23, 2019)

We analyzed numerically computed velocity autocorrelation functions and generalized frequency spectra of charge distribution in homogeneous DNA sequences at finite temperature. The autocorrelation function and generalized frequency spectrum (frequency-dependent diffusion coefficient) are phenomenologically introduced based on the functional of mean-square displacement of the charge in DNA. The charge transfer in DNA was modeled in the framework of the semi-classical Holstein model. In this model, DNA is represented by a chain of oscillators placed into thermostat at a given temperature that is provided by the additional Langevin term. Correspondence to the real DNA is provided by choice of the force parameters, which are calculated with quantum-chemical methods. We computed the diffusion coefficient for all homogenous DNA chains with respect to the temperature and found a special scaling of independent variables that the temperature dependence of the diffusion coefficient for different homogenous DNA is almost similar. Our calculations suggest that for all the sequences, only one parameter of the system is mainly responsible for the charge kinetics. The character of individual motions contributing to the charge mobility and temperature-dependent regimes of charge distribution is determined.

Key words and phrases: charge transfer, velocity autocorrelation function, generalized frequency spectrum, DNA, Holstein model

1. Introduction

Kinetics of charge transfer in polarized one-dimensional chains at finite temperature is an attractive and pressing theoretical problem by itself [1]–[4].

Its particular importance is related to the discovery of conducting properties in DNA [5]–[7]. On the first hand, this transfer may determine the biological functions of DNA. On the second hand, this opens up fresh opportunities in nanobioelectronics [8]–[10].

A basic qualitative simulation of charge transfer in DNA is a pioneered Holstein model for describing the charge transfer process in one-dimensional chains [11]. In the semi-classical approximation, DNA nucleotide pairs are modeled by a sequence of unconnected oscillators arranged in a chain [12]. A charge travels along a chain in the strong coupling approximation. Motions of the sites influence the charge propagation, and conversely, the charge probability density affects the charge motion.

The Holstein model is rather simple and can hardly describe the charge propagation in DNA realistically. Nevertheless, it is nonlinear and demonstrates different regimes. The study of this model can give qualitative insight into the nature of charge transfer in one-dimensional chains, including biological polymers.

The Holstein model is thoroughly investigated. Numerous papers are devoted to the analytical and numerical analysis of the original quantum model and its semi-classical approximation. However, the charge transfer kinetics at finite temperature is still to be understood. Of importance in this respect is the diffusion coefficient of a charge. Earlier, we studied its temperature dependence inhomogeneous chains of different nucleotide structures and found the scales which mainly determine differences in the charge diffusion in different chains [13].

This work continues the earlier started analysis. In order to better appreciate the kinetics of an added charge propagation along an infinite homogeneous chain, find all the motions which contribute into its mobility and determine the diffusion coefficient, we calculate and analyze autocorrelation functions of the charge propagation velocities and a relevant generalized frequency spectrum which is a frequency-dependent diffusion coefficient. We show that the earlier suggested scale is natural for the model, and the diffusion coefficients differ only in the low-frequency range for different sequences. In the limit of high and low temperatures, the nucleotide structure is irrelevant. Analysis of autocorrelation functions suggests that the charge propagation is contributed by dissipation and reflection at long distances as well as reflections from neighboring sites. As the temperature grows, these motions arise, coexist, and alternate. In the limit of finite temperature, the charge diffusion ceases.

A detailed straightforward analysis of the Holstein model kinetics at finite temperature requires direct numerical simulation concerned with a vast amount of computations. Determinate time dependencies should be identified from chaotic trajectories by averaging a large number of such trajectories. An essential tool to accomplish these ends is our unique method [14], [15], which enables speeding up calculations by three orders of magnitude as compared to difference schemes. The approach implies combining Magnus expansion methods used to reveal a charge evolution with a stochastic difference scheme applied to calculate motion trajectories of classical sites. This computational method enabled us to model reasonably sized samples so that to calculate a velocity autocorrelation function smooth enough to be subsequently analyzed.

2. Theory

2.1. Discrete Holstein model in semi-classical approximation. Modelling a thermostat

The charge transfer in a one-dimensional double-strand chain will be considered in the framework of the Holstein model. An electron travels along a chain whose sites are modeled by unconnected classical harmonical oscillators. The model Hamiltonian reads:

$$\hat{H} = \sum_{n,m} \nu_{nm} |n\rangle \langle m| + \alpha \sum_{n} q_n |n\rangle \langle n| + \sum_{n} \frac{1}{2} K q_n^2 + \sum_{n} \frac{1}{2} M \dot{q_n}^2, \quad (1)$$

where ν_{nm} are matrix elements or energies of electron transitions between the sites n and m, α is a constant of electron coupling with displacement of the n-th site q_n, M and K are mass and elasticity coefficient of the oscillators, respectively.

We will deal with homogeneous chains in the nearest neighbor approximation:

$$\nu_{nm} = \nu \delta_{n,m\pm 1}.$$

If we seek a solution corresponding to Hamiltonian (1), in the form

$$|\Psi\rangle = \sum_{n} b_n (t) |n\rangle ,$$

then the relevant Schroedinger equation for a charge and the equation for the sites motion at finite temperature is written as:

$$i\hbar \frac{db_n}{dt} = \nu (b_{n-1} + b_{n+1}) + \alpha q_n b_n, \quad (2a)$$

$$M \frac{d^2 q_n}{d^2 t} = -K q_n - \alpha |b_n|^2 + \Gamma \frac{dq_n}{dt} + A_n (t) . \quad (2b)$$

To model the temperature of the surrounding medium we place the chain in a Langevin thermostat. For this purpose equation for classical sites (2b) will include a term with friction (where Γ is a friction coefficient) and a random force $A_n (t)$ with a normal distribution and the autocorrelation function:

$$\langle A_n (t) A_m (t') \rangle = 2\Gamma k_B T \delta_{n,m} \delta (t - t') ,$$

where T is temperature and k_B is the Bolzmann constant.

2.2. Change-over to dimensionless parameters. Scaling of autocorrelation functions

If we neglect the influence of quantum equation (2a) on classical equation (2b), the latter becomes a Langevin-type equation, and the solutions do not depend on the charge distribution over the chain. In paper [16], we called this variant of the system an "adiabatic approximation". In the complete system, the quantum subsystem affects classical displacements but to a limited extent.

Therefore we explicitly separate a temperature multiplier in front of them, proceeding from the expression for dispersion of the oscillator coordinate q_n with the elasticity coefficient K:

$$\langle q_n^2 \rangle = \frac{k_B T}{K}.$$

This expression follows from virial theorem and determines the scale of variation of a classical oscillator amplitude as a function of temperature:

$$q_n = \sqrt{\frac{k_B T}{K}} u_n.$$

The time scale specifies the matrix element $t = \tau\hbar/\nu$. Let us rewrite equations (2) with regard to the chosen scales in dimensionless form:

$$i\frac{db_n}{d\tau} = b_{n-1} + b_{n+1} + \theta u_n b_n, \tag{3a}$$

$$\frac{d^2 u_n}{d\tau^2} = -\omega_0^2 u_n - \frac{\chi}{\theta}|b_n|^2 + \gamma\frac{du_n}{d\tau} + Z_n(\tau), \tag{3b}$$

$$\langle Z_n(\tau) Z_n(\tau') \rangle = 2\gamma\omega_0^2 \delta(\tau - \tau'),$$

where

$$\omega_0 = \frac{\hbar}{\nu}\sqrt{\frac{K}{M}}, \quad \gamma = \frac{\hbar}{\nu}\frac{\Gamma}{M}, \quad \chi = \alpha^2\frac{\hbar^2}{\nu^3 M}, \quad \theta = \frac{\alpha}{\nu}\sqrt{\frac{k_B T}{K}}.$$

The quantum equation contains only one dimensionless parameter θ, which is the amplitude multiplier of classical displacements. It is mainly responsible for the influence of the classical subsystem on the quantum one, depending on temperature. This fact suggests that the electron distribution kinetics may mainly depend on θ for all chain sequences. In particular, the influence of the classical system becomes negligible for $\theta \to 0$, and the dependence on the nucleotide sequence completely disappears. Our results demonstrate that this choice of the scale is appropriate.

Apart from frequency ω_0 and friction γ, responsible for oscillator motion characteristics, the classical equation involves a parameter χ/θ, which determines a reverse influence of the quantum subsystem on the classical one. Analysis of χ/θ suggests that this influence is neglectable for high temperatures. Besides, we also can neglect it in the case of nucleotide chains with a large matrix element ν. If we set a constant $\chi = 0$ for these cases, we obtain an adiabatic approximation considered earlier in [16].

2.3. Charge mean-square displacement and generalized frequency spectrum

The kinetic properties of stochastic system (3) are described by the velocity autocorrelation function and the generalized frequency spectrum. These

functions can be calculated from the density of probability of finding an electron at site n in a chain of length $2N+1$:

$$P(n,\tau) = b_n(\tau)\, b_n^*(\tau).$$

In the semi-classical approximation the root-mean-square displacements in dimensionless form are calculated by the formula:

$$\langle x^2 \rangle = \xi(\tau) = \sum_{n=-N}^{N} n^2 P(n,\tau). \tag{4}$$

Then the diffusion coefficient can be found as a slope of the curve $\xi(\tau)$ on its linear segment or as an asymptotic value of the derivative of the displacement with respect to time $\eta(\tau) = \xi(\tau)'$, or via the integral of the second derivative of the displacement with respect to time $\psi(\tau) = \xi(\tau)''$. We will call this coefficient a static one and denote it as $D(0)$:

$$D(0) = \frac{1}{2}\int_0^\infty \psi(\tau)\, d\tau.$$

The natural generalization of the static diffusion coefficient is a frequency-dependent diffusion coefficient $D(\phi)$, which can be found as a generalized frequency spectrum of the second derivative of the displacement function with respect to time:

$$D(\phi) = \frac{1}{2}\int_0^\infty \psi(\tau)\cos(2\pi\phi\tau)\, d\tau, \tag{5}$$

where ϕ is dimensionless frequency which is related to frequency in hertz (f) as:

$$f = \frac{\nu}{\hbar}\phi = 2\pi\frac{\nu}{h}\phi.$$

Function $\psi(\tau)$ in semi-classical approximation is a velocity autocorrelation function.

3. Results and discussion

At the initial moment a charge was inserted in the center of a homogeneous chain of length $2N+1$ with temperature distribution of the degrees of freedom of harmonical oscillators:

$$b_n(0) = \delta_{n,0}, \quad \frac{du_n}{d\tau}(0) = \mathcal{N}(0,1), \quad u_n(0) = \mathcal{N}(0,1), \tag{6}$$

where $\delta_{i,j}$ is Kronecker delta, $\mathcal{N}(\mu,\sigma)$ is a normal distribution with the mean μ and dispersion σ^2.

The trajectory of the system motion was calculated from initial states (6), each time with new values of u_n and $\dot{u}_n$. The calculations were carried out by the method, which combines Magnus expansion with a stochastic difference scheme [14], [15]. For the trajectories to correspond to charge propagation

along an infinite chain, the chain length N was chosen such that during the time of modeling the front of propagation of the charge probability density would not come up to its end.

Then we calculated the second derivative of the root-mean-square displacement with respect to (3), (4) by averaging over samples. After that, we found the frequency spectrum by formula (5) using the fast cosine transform.

We chose the parameters listed in Table 1 as in our previous work [13]. These parameters are typical for DNA.

Table 1

Dimensional parameters of the Holstein model for dsDNA

$M = 10^{-21}$ g	$K = 0.062$ eV/Å^2	$\Gamma = 6 \cdot 10^{-10}$ g/s	$\alpha = 0.13$ eV/Å
$\nu_A = 0.030$ eV	$\nu_C = 0.041$ eV	$\nu_G = 0.084$ eV	$\nu_T = 0.158$ eV

We repeated the calculations for a set of temperatures and homogeneous dsDNA chains composed of different nucleotides. Table 2 lists dimensionless parameters.

Table 2

Dimensionless parameters for dsDNA as a function of a nucleotide sequence

parameter	poly A	poly C	poly G	poly T
ω_0	0.02193	0.01605	0.007837	0.004167
γ	0.01316	0.009631	0.004702	0.0025
χ	0.004219	0.001654	1.925×10^{-4}	2.894×10^{-5}

A common property of the velocity autocorrelation functions at any temperature is that they are equal to 4 in the small area after an initial time instant. This value corresponds to the velocity of the ballistic motion at zero temperature, which is equal to 2. A comparison of autocorrelation functions for chains composed of different nucleotides suggests that for the same value of θ, the functions differ only in the attenuation asymptotics. The spectra demonstrate differences at low frequencies for finite values of θ and, accordingly, different diffusion coefficients $D(0)$ (see Figure 1, dashed lines). Here we use the scale were these differences are insignificant. In particular, they lack in the limit of low and high temperatures.

Earlier in work [13], we carried out a more detailed analysis of the temperature dependencies of the static diffusion coefficient for homogeneous dsDNA chains with different nucleotide sequences and suggested the scales in which the temperature dependencies of $D(0)$ are close for chains with different sequences. Analyzing the spectra in this scale here, we see that differences in the frequency-dependent diffusion coefficient blend as the frequency is increasing, and virtually disappear at the frequency, where an absolute maximum of the spectrum is observed (see Figure 1, solid lines).

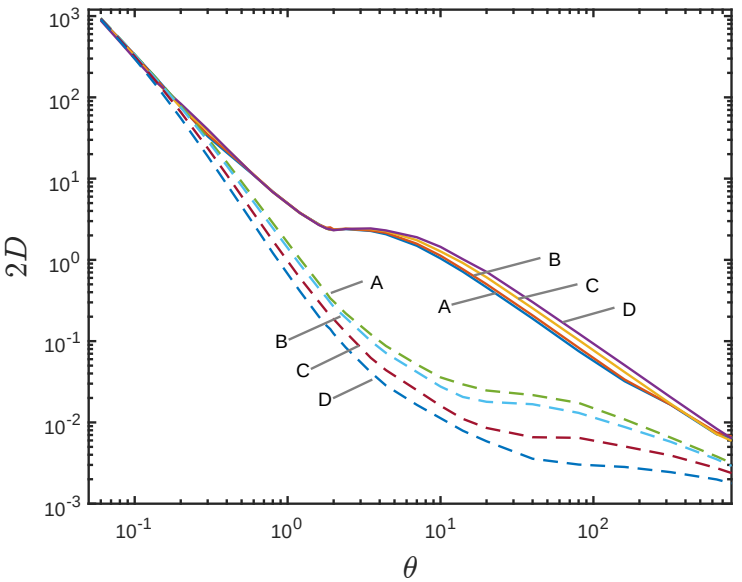

Figure 1. Temperature dependencies of the frequency-dependent coefficient; A, Poly A dsDNA; B, Poly C dsDNA; C, Poly G dsDNA; D, Poly T dsDNA. Dashed lines for the dependencies of $2D(0)$ on θ; solid lines for the dependencies of $(\max 2D(\omega))_\theta$ on θ

As the temperature changes, the form of autocorrelation functions and spectra change too. Their analysis enables us to identify four different regimes. Since we have shown that any differences between the chains with different nucleotide structures are insignificant in our scale, and their character is determined, we will deal only with Poly A dsDNA chains in what follows. In the limit of infinitely small temperatures, the autocorrelation function tends to attenuate exponent:

$$\psi(\tau) = \psi(0)\, e^{-\tau/\tau_0}.$$

Its generalized frequency spectrum has an analytical form similar to that of the real part of the frequency-dependent conductivity, according to Drude formula:

$$D(\phi) = \frac{\psi(0)\,\tau_0}{1 + 4\pi^2\phi^2\tau_0^2}.$$

In accordance with fluctuation-dissipative theorem, the mobility $\mu(\omega)$ is related to $D(\omega)$ as [17]:

$$\mu(2\pi\phi) = \frac{e}{T} D(2\pi\phi).$$

The dependence of $\mu(0)$ on temperature is given in [18].

Notice also that the maximum of the frequency-dependent diffusion coefficient and, accordingly, the mobility at the relevant frequency is greater than the static diffusion coefficient (see Figure 1). It suggests that DNA can serve as a conductor of alternating current.

In the range of extra-low temperatures for near-zero θ, the autocorrelation functions and the spectra keep monotonously attenuating (see Figure 2) until

the dimensionless parameter θ reaches the value $\theta = 0.14$ in Poly T dsDNA or $\theta = 0.3$ in Poly A dsDNA. This boundary is slightly different for chains with different nucleotide sequences (see Figure 1). For the first regime, scattering at long distances exceeding one site on the average is typical.

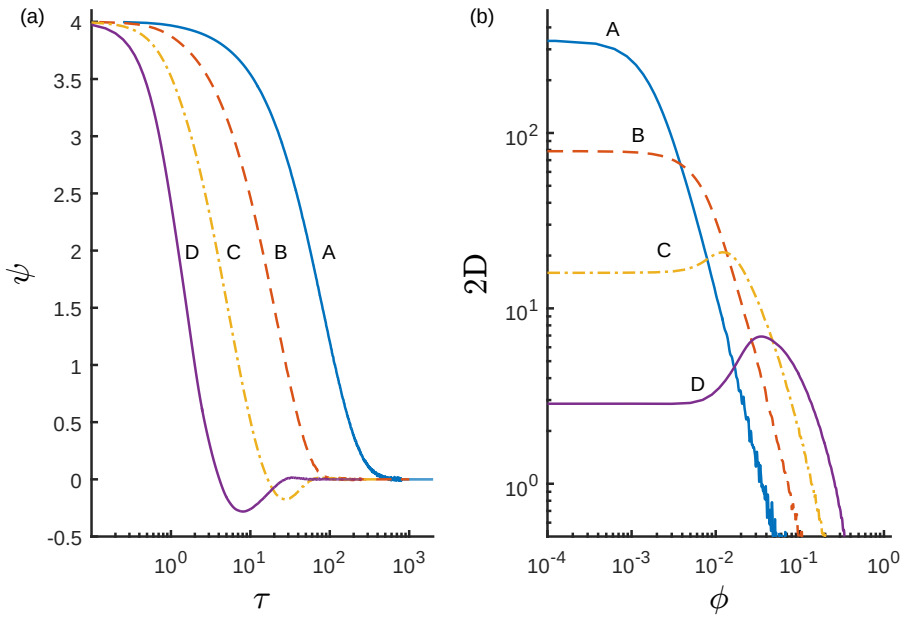

Figure 2. (a) Velocity autocorrelation functions and (b) generalized frequency spectrum of the charge propagation along Poly A dsDNA in the range of low and extra-low temperatures; A, $\theta = 0.1$; B, $\theta = 0.2$; C, $\theta = 0.4$; D, $\theta = 0.8$

In the range of low temperatures, until the dimensionless parameter becomes $\theta = 1$, reflection at long distances arises. In this regime, the velocity autocorrelation function (see Figure 2(a)) is not monotone and has a single minimum in the negative range. The absolute value of the minimum increases with growing θ, while its coordinate decreases. Now the spectra demonstrate a low-frequency maximum whose frequency increases with growing θ, while the value decreases (see Figure 2(b)).

Then, up to the value of $\theta = 3.5$, a range of moderate temperatures is observed. In this temperature range a high-frequency maximum caused by oscillations of the autocorrelation function $\psi(\tau)$ occurs after the first minimum (see Figure 3(a)). At the same time, the absolute value of the first minimum of the autocorrelation function keeps growing. High-frequency oscillations arise while the function attenuates after the first minimum. Thus, in the range of moderate temperatures, reflection at long distances, and reflection from neighboring sites coexist.

Looking at the spectrum $2D(\omega)$, we see that the low-frequency maximum keeps decreasing, while its frequency decreases and approaches the frequency of the second maximum (Figure 3(b)). The position of the high-frequency peak on the spectrum is independent of temperature. The first and the second maxima of the spectrum are well seen and have nearly the same value for $\theta = 1.9$ (see the inset in Figure 3(b)).

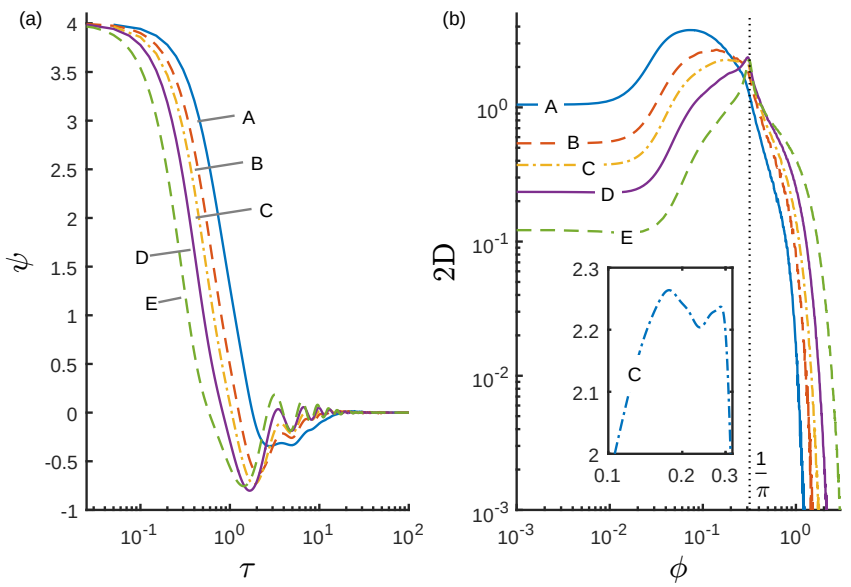

Figure 3. (a) Velocity autocorrelation functions and (b) generalized frequency spectrum of the charge propagation along Poly A dsDNA in the range moderate temperatures; A, $\theta = 1.2$; B, $\theta = 1.6$; C, $\theta = 1.9$; D, $\theta = 2.4$; E, $\theta = 3.5$

Notice that the value of the parameter $\theta = 1.9$ for which the high-frequency peak is approximately equal in value to the low-frequency one is the same for different types of chains, which is confirmed by the curves of the maxima shown in Figure 1. The value of the parameter θ for which the low-frequency maximum of the spectrum disappears while the high-frequency one emerges can reasonably be called a critical value. Dimensional critical temperatures corresponding to the critical parameter are listed in Table 3 for different types of chains.

Table 3
Critical temperature for $\theta = 1.9$ and position of high-frequency peak for different nucleotide sequences

	units	poly A	poly C	poly G	poly T
f_p	THz	14.5	19.8	40.6	76.4
T_c	° C	−134.76	−14.68	811.80	3565.37

Regularity and homogeneity of the chain cause the high-frequency peak. It occurs at a frequency of $\phi = 1/\pi$. The dimension frequency depends only on matrix element:

$$f_p = 2\frac{\nu}{h}.$$

The values of this peak frequency for the different nucleotide sequences are presented in Table 3. Obviously, in the case of inhomogeneous regular chains,

these frequencies will be more than one, and the spectra will contain several relevant peaks.

In the range of high temperatures, motion mainly fulfills as hopping between neighboring sites. As distinct from the previous regimes, the absolute value of the first minimum of the autocorrelation function decreases here with growing θ (see Figure 4(a)). A decrease of its coordinate is considerably retarded and tends to 1. At the same time, the initial attenuation occurs more sharply. Initially, the function sharply decreases to zero and then slowly goes to the first minimum. Oscillations of the autocorrelation function in this regime occur about the abscissa axis rather than about the low-frequency envelope.

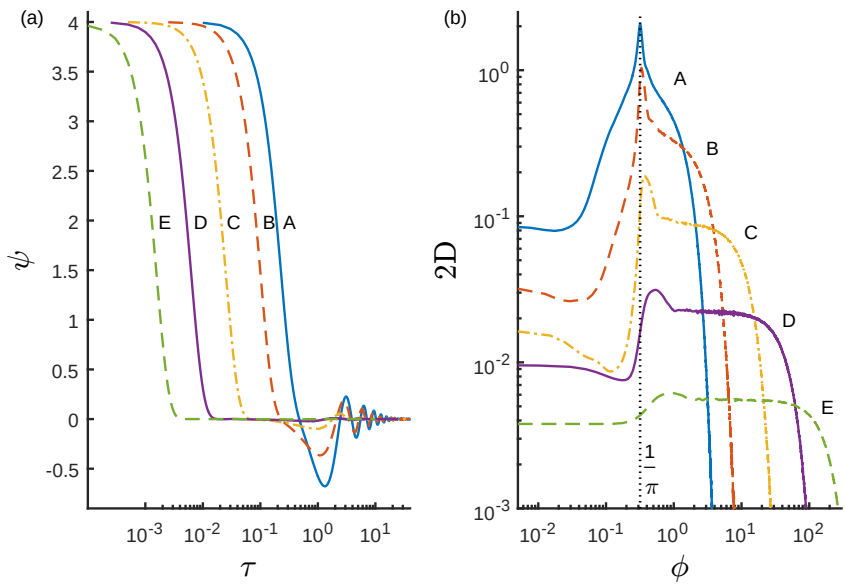

Figure 4. (a) Velocity autocorrelation functions and (b) generalized frequency spectrum of the charge propagation along Poly A dsDNA in the range of high and ultrahigh temperatures; A, $\theta = 4.4$; B, $\theta = 10$; C, $\theta = 40$; D, $\theta = 160$; E, $\theta = 640$

The spectrum demonstrates only a high-frequency peak, which decreases with growing θ (see Figure 4(b)). The spectrum smoothly widens.

Obviously, in the limit of high temperatures, the spectrum widens and becomes monotone. The charge propagation ceases.

As is seen from Figures 2–4, for rather high ω, at any temperatures, except for extra-low and superhigh ones, $D(\omega)$ increases with growing temperature. This effect is known for static disorder [17].

4. Conclusion

We considered the frequency spectra of the diffusion coefficient (mobility) of an excess charge in a Holstein molecular chain for different temperatures.

We revealed the character of motions contributing to the charge diffusion in the Holstein model. The presence of temperature causes a dynamical disorder even in an ideal chain. Let us call the main differences between the frequency dependencies of chains with static disorder and those with

the dynamic disorder caused by temperature fluctuations. In the static case, the diffusion coefficient increases with growing frequency [17], while in the dynamic case, more complicated behavior is observed (see Figures 2–4). We demonstrated the existence of asymptotics at low and high temperatures. For finite temperatures, we identified four temperature ranges in which autocorrelation functions and their spectra have similar peculiarities/features. Accordingly, the charge diffusion inside these ranges demonstrates the same character. The character is changing in passing to a different temperature range. Low temperatures cause weak scattering without reflections, as a result of which the ballistic motion changes for the diffusion one. As the temperature increases, at first, a reflection at long distances emerges, then it is added with reflections from neighboring sites. Both these motions slow down the charge diffusion. In the limit of high temperatures, the motion degenerates into hopping between neighboring sites, and the charge diffusion ceases.

We revealed the character of motions contributing to the charge diffusion in the Holstein model.

All the results are presented in dimensionless values, which enabled us to identify the main parameters and recognize the different regimes.

The autocorrelation functions in themselves, as well as their spectra, are also a significant result. Their calculation was made possible only with the use of special unique methods of numerical integration of differential equations.

Presently, DNA is considered to be a promising material for constructing molecular wires. However, even homogeneous synthetic nucleotide chains at room temperatures demonstrate deficient mobility in the case of direct current [19], [20]. A possible solution to this problem, according to the results obtained, is the use of not direct but alternating current of rather high frequency.

Acknowledgments

This article is published on the basis of preprint [21].

References

[1] P. Maniadis, G. Kalosakas, K. Ø. Rasmussen, and A. R. Bishop, "AC conductivity in a DNA charge transport model," *Physical Review E*, vol. 72, p. 021 912, 2 Aug. 2005. DOI: 10.1103/PhysRevE.72.021912.

[2] G. L. Goodvin, A. S. Mishchenko, and M. Berciu, "Optical conductivity of the Holstein polaron," *Physical Review Letters*, vol. 107, p. 076 403, 7 Aug. 2011. DOI: 10.1103/PhysRevLett.107.076403.

[3] L. D. Siebbeles and Y. A. Berlin, "Quantum motion of particles along one-dimensional pathways with static and dynamic energy disorder," *Chemical Physics*, vol. 238, no. 1, pp. 97–107, 1998. DOI: 10.1016/S0301-0104(98)00311-5.

[4] P. Prins, F. C. Grozema, J. M. Schins, and L. D. A. Siebbeles, "Frequency dependent mobility of charge carriers along polymer chains with finite length," *Physica Status Solidi B*, vol. 243, no. 2, pp. 382–386, 2006. DOI: 10.1002/pssb.200562719.

[5] C. J. Murphy, M. R. Arkin, Y. Jenkins, N. D. Ghatlia, S. H. Bossmann, N. J. Turro, and J. K. Barton, "Long-range photoinduced electron transfer through a DNA helix," *Science*, vol. 262, no. 5136, pp. 1025–1029, 1993. DOI: 10.1126/science.7802858.

[6] P. O'Neill, A. W. Parker, M. A. Plumb, and L. D. A. Siebbeles, "Guanine modifications following ionization of DNA occurs predominantly via intra- and not interstrand charge migration: an experimental and theoretical study," *Journal of Physical Chemistry B*, vol. 105, no. 22, pp. 5283–5290, 2001. DOI: 10.1021/jp003514t.

[7] G. I. Livshits *et al.*, "Long-range charge transport in single G-quadruplex DNA molecules," *Nature Nanotechnology*, vol. 9, no. 12, pp. 1040–1046, 2014. DOI: 10.1038/nnano.2014.246.

[8] V. D. Lakhno, "DNA nanobioelectronics," *International Journal of Quantum Chemistry*, vol. 108, no. 11, pp. 1970–1981, 2008. DOI: 10.1002/qua.21717.

[9] T. Chakraborty, *Charge migration in DNA: perspectives from Physics, Chemistry, and Biology*, ser. NanoScience and Technology. Springer Berlin Heidelberg, 2007.

[10] A. Offenhäusser and R. Rinaldi, Eds., *Nanobioelectronics – for Electronics, Biology, and Medicine*. Springer, New York, 2009, 337 pp.

[11] T. Holstein, "Studies of polaron motion," *Annals of Physics*, vol. 8, no. 3, pp. 325–342, 1959. DOI: 10.1016/0003-4916(59)90002-8.

[12] N. S. Fialko and V. D. Lakhno, "Nonlinear dynamics of excitations in DNA," *Physics Letters A*, vol. 278, pp. 108–111, 1–2 2000. DOI: 10.1016/S0375-9601(00)00755-6.

[13] D. A. Tikhonov, N. S. Fialko, E. V. Sobolev, and V. D. Lakhno, "Scaling of temperature dependence of charge mobility in molecular Holstein chains," *Physical Review E*, vol. 89, p. 032 124, 3 Mar. 2014. DOI: 10.1103/PhysRevE.89.032124.

[14] E. V. Sobolev, D. Tikhonov, and N. S. Fialko, "About Numerical solution of the Holstein's discrete model [O chislennom reshenii uravneniy diskretnoy modeli Kholsteyna]," in *Proceedings of the XIX All-Russian Conference "Theoretical bases and generation of numerical algorithms of solving mathematical physics problems", devoted to K. I. Babenko, Durso, Russia, 2012*, in Russian, Moscow: Keldysh Institute of Applied Mathematics, 2012, p. 90.

[15] E. V. Sobolev, D. Tikhonov, and N. S. Fialko, "Numerical solution of the Holstein's discrete model in the problem of charge transfer in DNA [Chislennoye resheniye uravneniy diskretnoy modeli Kholsteyna v zadache o modelirovanii perenosa zaryada v DNK]," in *Proceedings of the 4th International Conference on Mathematical Biology and Bioinformatics, Pushchino, Russia, 2012*, V. D. Lakhno, Ed., in Russian, Moscow: MAKS Press, 2012, p. 18.

[16] D. A. Tikhonov, E. V. Sobolev, V. D. Lakhno, and N. S. Fialko, "Adiabatic approximation for the calculation of the charge mobility in the DNA Holstein model [Adiabaticheskoye priblizheniye pri raschetakh podvizhnosti zaryada v kholsteynovskoy modeli DNK]," *Matematicheskaya biologiya i bioinformatika*, vol. 6, no. 2, pp. 264–272, 2011, in Russian. DOI: 10.17537/2011.6.264.

[17] J. C. Dyre and T. B. Schrøder, "Universality of AC conduction in disordered solids," *Reviews of Modern Physics*, vol. 72, pp. 873–892, 3 Jul. 2000. DOI: 10.1103/RevModPhys.72.873.

[18] V. D. Lakhno and N. S. Fialko, "Bloch oscillations in a homogeneous nucleotide chain," English, *JETP Letters*, vol. 79, no. 10, pp. 464–467, 2004. DOI: 10.1134/1.1780553.

[19] D. M. Basko and E. M. Conwell, "Effect of solvation on hole motion in DNA," *Physical Review Letters*, vol. 88, p. 098 102, 9 Feb. 2002. DOI: 10.1103/PhysRevLett.88.098102.

[20] V. D. Lakhno and N. S. Fialko, "Solvation effects on hole mobility in the poly G/Poly C duplex," *Russian Journal of Physical Chemistry A*, vol. 86, no. 5, pp. 832–836, 2012. DOI: 10.1134/S0036024412050196.

[21] D. A. Tikhonov, E. V. Sobolev, and V. D. Lakhno, "Charge diffusion in homogeneous molecular chains based on the analysis of generalized frequency spectra in the framework of the Holstein model," Tech. Rep. 70-e, 2018, pp. 1–16. DOI: 10.20948/prepr-2018-70-e.

For citation:

D. A. Tikhonov, E. V. Sobolev, V. D. Lakhno, Charge diffusion in homogeneous molecular chains based on the analysis of generalized frequency spectra in the framework of the Holstein model, Discrete and Continuous Models and Applied Computational Science 27 (3) (2019) 217–230. DOI: 10.22363/2658-4670-2019-27-3-217-230.

Information about the authors:

Dmitry A. Tikhonov (Russian Federation) — Candidate of Physical and Mathematical Sciences, Senior researcher, Institute of Mathematical Problems of Biology Branch of Keldysh Institute of Applied Mathematics Russian Academy of Sciences (e-mail: dmitry.tikhonov@gmail.com, phone: +7(915)4013703, ORCID: https://orcid.org/0000-0002-1779-464X, ResearcherID: O-2214-2013, Scopus Author ID: 7006659212)

Egor V. Sobolev (Germany) — Candidate of Physical and Mathematical Sciences, Postdoctoral fellow, European Molecular Biology Laboratory, Hamburg Unit (e-mail: egor@embl-hamburg.de, phone: +49(4089)902184, ORCID: https://orcid.org/0000-0003-2478-5685, ResearcherID: O-2216-2013, Scopus Author ID: 55971569900)

Victor D. Lakhno (Russian Federation) — Doctor of Physical and Mathematical Sciences, Scientific Director, Institute of Mathematical Problems of Biology Branch of Keldysh Institute of Applied Mathematics Russian Academy of Sciences (e-mail: lak@impb.ru, phone: +7(4967)318504, ORCID: https://orcid.org/0000-0001-9224-769X, ResearcherID: N-7346-2013, Scopus Author ID: 7003392437)

УДК 519.6
DOI: 10.22363/2658-4670-2019-27-3-217-230

О диффузии заряда в однородных молекулярных цепочках на основе анализа обобщенных частотных спектров в рамках модели Холстейна

Д. А. Тихонов[1,2], **Е. В. Соболев**[1,3], **В. Д. Лахно**[1]

[1] *Институт математических проблем биологии (ИМПБ РАН)*
ул. проф. Виткевича, д. 1, г.Пущино, Московская область, 142290, Россия
[2] *Институт теоретической и экспериментальной биофизики РАН*
ул. Институтская, д. 3, г. Пущино, Московская область, 142290, Россия
[3] *Европейская лаборатория молекулярной биологии, отделение в Гамбурге*
с/о DESY, д. 25A, Ноткештрассе 85, 22607 Гамбург, Германия

В статье проведён анализ автокорреляционных функций скорости и обобщённых частотных спектров распространения заряда в однородных последовательностях ДНК при конечной температуре. Функции рассчитаны численно в рамках квазиклассической модели Холстейна. Показано, что в системе только один параметр главным образом определяет кинетику заряда для всех последовательностей. Анализ позволил определить характер отдельных движений, вносящих вклад в подвижность заряда, и выделить различные режимы распространения заряда в зависимости от температуры.

Ключевые слова: перенос заряда, автокорреляционная функция скорости, обобщённый частотный спектр, ДНК, модель Холстейна

Research article

UDC 524, 531
PACS 04.20.−q, 04.20.Dw
DOI: 10.22363/2658-4670-2019-27-3-231-241

Geodesic motion near self-gravitating scalar field configurations

Ivan M. Potashov, Julia V. Tchemarina, Alexander N. Tsirulev

Faculty of Mathematics
Tver State University
35 Sadovy Pereulok, Tver 170002, Russian Federation

(received: December 12, 2019; accepted: December 23, 2019)

We study the geodesics motion of neutral test particles in the static spherically symmetric spacetimes of black holes and naked singularities supported by a self-gravitating real scalar field. The scalar field is supposed to model dark matter surrounding some strongly gravitating object such as the centre of our Galaxy. The behaviour of timelike and null geodesics very close to the centre of such a configuration crucially depends on the type of spacetime. It turns out that a scalar field black hole, analogously to a Schwarzschild black hole, has the innermost stable circular orbit and the (unstable) photon sphere, but their radii are always less than the corresponding ones for the Schwarzschild black hole of the same mass; moreover, these radii can be arbitrarily small. In contrast, a scalar field naked singularity has neither the innermost stable circular orbit nor the photon sphere. Instead, such a configuration has a spherical shell of test particles surrounding its origin and remaining in quasistatic equilibrium all the time. We also show that the characteristic properties of null geodesics near the centres of a scalar field naked singularity and a scalar field black hole of the same mass are qualitatively different.

Key words and phrases: geodesic, black hole, naked singularity, scalar field

1. Introduction

In recent years new astrophysical observations give us convincing evidence for the presence of strongly gravitating objects in the center of most of normal galaxies. These objects are commonly identified with supermassive black holes, but the modern astrophysical data are not quite enough to exclude other possibilities, such as naked singularities, boson stars, and wormholes. For example, the shadow in the centre of the galaxy M87 and the real image of the photon ring around the shadow, observed by the Event Horizon Telescope collaboration this year, have been immediately interpreted as the existence of the photon sphere and, consequently, the event horizon [1]. However, it is shown in Ref. [2] within a simple model that a naked singularity can also have

both the shadow and the photon sphere. In fact, a natural way to distinguish between the different types of the gravitating objects is to explore spacetime geometry through the study (both observationally and theoretically) of the motion of test particles and light rays near the centres of galaxies [3]–[5].

The observational efficiency directly depends on a model in which the astrophysical data for the central objects will be interpreted. First, one should not think of the central objects in galaxies as being in vacuum, because dark matter is mainly concentrated around them. Another problem is that the nature of dark matter and its distribution near galactic centres remain unknown at present. This means that a meaningful interpretation of the observations should be based on an appropriate mathematical model of the central regions: we model dark matter by a nonlinear scalar field which is assumed to be minimally coupled to gravity. Our aim is to compare the behaviour of timelike and null geodesics for a scalar field black hole and a scalar field naked singularity of the same mass. For such configurations, the general properties of timelike geodesics were studied in Refs. [6]–[8]. In this paper, we focus our attention on the comparison of bound trajectories of massive test particles and light rays in the immediate vicinity of the centres of scalar field black holes and scalar field naked singularities.

The paper is organised as follows. In Section 2 we describe the necessary mathematical background for static, spherically symmetric scalar field configurations restricting our attention to the case of the minimal coupling between curvature and a real scalar field. In Section 3 we discuss general features of bound and unbound orbits of free neutral massive and massless particles. In Section 4 we consider a simple example which illustrates some characteristic features of the photon orbits of scalar field black holes and scalar field naked singularities in comparing with the orbits of massive test particles.

In this paper, we use the geometrical system of units with $G = c = 1$ and adopt the metric signature $(+ - - -)$. In tensor notation, we use the summation convention over repeated indices, and Greek indices take the values $0, 1, 2, 3$.

2. Self-gravitating spherically symmetric scalar field configurations

We begin with the action

$$\Sigma = \frac{1}{8\pi} \int \left(-\frac{1}{2} R + \langle d\phi, d\phi \rangle - 2V(\phi) \right) \sqrt{|g|}\, d^4x \,,$$

where ϕ is a real scalar field, R is the scalar curvature, $V(\phi)$ is a self-interaction potential, and the angle brackets denote the scalar product with respect to the spacetime metric. The metric of a spherically symmetric spacetime in the Schwarzschild-like coordinates can be written in the form

$$ds^2 = A dt^2 - \frac{dr^2}{f} - r^2 (d\theta^2 + \sin^2\theta\, d\varphi^2),$$

where the metric functions A and f depend only on the radial coordinate r. For the metric function A, it is convenient to make the substitution

$$A(r) = f(r)\mathrm{e}^{2F(r)},$$

so that the Einstein-Klein-Gordon equations take the form

$$-\frac{f'}{r} - \frac{f-1}{r^2} = \phi'^2 f + 2V, \tag{1}$$

$$\frac{f}{r}\left(2F' + \frac{f'}{f}\right) + \frac{f-1}{r^2} = \phi'^2 f - 2V, \tag{2}$$

$$-f\phi'' - \frac{\phi'}{2}f' - \phi' f\left(F' + \frac{1}{2}\frac{f'}{f} + \frac{2}{r}\right) + \frac{dV}{d\phi} = 0\,, \tag{3}$$

where a prime denotes differentiation with respect to r.

By adding equations (1) and (2), we obtain

$$F' = r\phi'^2. \tag{4}$$

Now we can eliminate F' from the two other equations and, as a result, solve those in the form of quadratures [9]–[15]. For our goal, we will employ the integral formulae obtained in Ref. [13]:

A general static, spherically symmetric, asymptotically flat solution of equations (1)–(3) *with an arbitrary self-interaction potential is given by the quadratures*

$$F(r) = -\int_r^\infty \phi'^2 r dr\,, \quad \xi(r) = r + \int_r^\infty (1 - \mathrm{e}^F)\, dr\,, \tag{5}$$

$$A(r) = 2r^2 \int_r^\infty \frac{\xi - 3M}{r^4}\,\mathrm{e}^F dr\,, \quad f(r) = \mathrm{e}^{-2F}A\,, \tag{6}$$

$$\tilde{V}(r) = \frac{1}{2r^2}\left(1 - 3f + r^2\phi'^2 f + 2\,\mathrm{e}^{-F}\,\frac{\xi - 3M}{r}\right), \tag{7}$$

where the parameter M is the Schwarzschild mass.

It is important to stress that each solution of equations (1)–(3) satisfies these quadratures independently of the monotonicity of the field function.

In order to use these quadratures, we will work with a specially defined function $\xi(r)$ which must satisfy the asymptotic condition

$$\xi = r + O\,(1/r)\,, \quad r \to \infty, \tag{8}$$

and then will sequentially find the metric functions ($\mathrm{e}^F = \xi'$), the scalar field (by integrating (4)), the function $\tilde{V}(r)$, and the self-interaction potential $V(\phi) = \tilde{V}(r(\phi))$. This method is commonly known as 'the inverse problem method for self-gravitating scalar field configurations'. It is also important to stress that we consider the scalar field as a phenomenological model of dark matter rather than as a really existing fundamental field. Note that

we could include the cosmological constant in the potential as the additional term $\Lambda/2$, but its contribution to the geometry of the central region would be negligible. The absence of the cosmological constant simply means that $V(\phi(\infty)) = 0$. Therefore, the so-called 'no-hair theorem' is not essential in the current astrophysical context.

Using quadratures (5) and (6), we can write algebraically independent components of the curvature in the orthonormal basis, associated with the metric (2), in the form

$$R_{0101} = \phi'^2 f - \frac{f-1}{r^2}, \quad R_{2323} = \frac{f-1}{r^2}, \tag{9}$$

$$R_{0202} = R_{0303} = -\frac{f}{r^2} + \mathrm{e}^{-F}\frac{\xi - 3M}{r^3}, \tag{10}$$

$$R_{1212} = R_{1313} = \frac{f}{r^2} - \phi'^2 f - \mathrm{e}^{-F}\frac{\xi - 3M}{r^3}. \tag{11}$$

On the other hand, in spherically symmetric spacetimes, the Kretchmann invariant, $K = R_{\alpha\beta\gamma\delta}R^{\alpha\beta\gamma\delta}/4$, equals the sum of the squared curvature components and, therefore, diverges if at least one of the curvature components do. Thus, in this case K and the scalar curvature R diverge at $r = 0$ for all solutions with the exception of some specific ones satisfying the conditions

$$\xi(r) = 3M + \mathrm{e}^{F(0)}r + O\left(r^3\right), \quad f(0) = 1 + O\left(r^2\right), \quad r \to \infty.$$

In the generally accepted manner, we call a solution *a naked singularity* (*a black hole*) if K diverges at $r = 0$ and $f > 0$ for all $r > 0$ (respectively, $f = 0$ at some radius $r_h > 0$ and $f > 0$ for all $r > r_h$).

For a given nonzero scalar field $\phi(r)$, it follows directly from (5) that $\xi' = \mathrm{e}^F > 0$ for all $r > 0$ and $\xi(0) > 0$, so that the metric function A, given by the quadrature (6), passes through zero and becomes negative as $r \to 0$ if and only if $3M > \xi(0)$. In other words, the corresponding configuration of mass M will be a naked singularity or a black hole if and only if

$$0 < 3M < \xi(0) \ \text{(naked singularities)} \quad \text{or} \quad 3M > \xi(0) \ \text{(black holes)},$$

respectively. In what follows we deal only with 'generic' configurations and do not consider the special (fine-tuned) case $3M = \xi(0)$; the latter leads to a naked singularity or a regular solution.

The geometrical system of units ($G = c = 1$) does not fix a unit of length. On the other hand, the geodesic structure of spacetime is scale invariant at the classical level, and the solution (6)–(7) is invariant under the scale transformations

$$r \to r/\lambda, \quad M \to M/\lambda, \quad V \to \lambda^2 V, \qquad \lambda > 0,$$

so that we can use an arbitrary unit of length. By applying $\lambda = M$ in this transformation, we can take, as it is usually done in general relativity, the mass of a scalar field configuration as the current unit of length. Thus, without loss of generality, we suppose everywhere below that $M = 1$.

3. Geodesic motion around scalar field configurations

In all stationary spherically symmetric spacetimes we have the conserved energy and angular momentum of a test particle. Together with the constancy condition for the norm of the four-velocity, this implies the existence of three integrals of motion. For the metric (2) they can be written in the form

$$\frac{dt}{ds} = \frac{E}{A}, \quad \frac{d\varphi}{ds} = \frac{J}{r^2}, \quad \left(\frac{dr}{ds}\right)^2 = \mathrm{e}^{-2F}\left(E^2 - V_{\text{eff}}\right), \tag{12}$$

$$V_{\text{eff}} = A\left(k + \frac{J^2}{r^2}\right), \tag{13}$$

where $V_{\text{eff}}(r)$ is the effective potential, E and J are, respectively, the specific energy and the specific angular momentum of a test particle, and $k = 0$ or $k = 1$ depending on whether we are considering null or timelike geodesics; for null geodesics, s is an arbitrary geodesic parameter, but not the interval.

For any asymptotically flat spacetime and for any value of J, $V_{\text{eff}} \to 0$ or $V_{\text{eff}} \to 1$ as $r \to \infty$ depending on whether $k = 0$ or $k = 1$, respectively. Another difference between null and timelike geodesics which is more interesting is that the behaviour of a null geodesic effectively depends only on the impact parameter b, so that

$$\left(\frac{dr}{ds}\right)^2 = E^2\mathrm{e}^{-2F}\left(1 - b^2\frac{A^2}{r^2}\right), \quad b = \frac{J}{E}, \tag{14}$$

where the coefficient E^2 on the right hand side can be eliminated by redefining the parameter: $\lambda = sE$.

It is shown in Ref. [8] that for a scalar field black hole spacetime, defined by the quadratures (5)–(7) and the conditions (8) and $3M > \xi(0)$, the lapse function $A(r)$ is a strictly increasing function outside the event horizon. In contrast, for a naked singularity spacetime, satisfying the conditions (8) and $3M < \xi(0)$, $A(r)$ necessarily has at least one minimum in the region $0 < r < \infty$. These properties give us a key distinguishing feature for the two types of scalar field configurations: they cause different behaviours of bound orbits close to the centre. The various numerical simulations with scalar field black hole solutions allow us to conclude that the radius of the corresponding innermost stable circular orbit, which is an important observational characteristic for black holes, is of order $3r_{_h}$ (analogously to the vacuum case). On the contrary, a scalar field naked singularity has no innermost stable circular orbit but has a unique degenerated *static orbit*, which has $J = 0$ and is located at $r = r_0$, where r_0 is the unique solution of the equation $A'(r) = 0$. From the point of view of a distant observer resting relative to the centre, a test particle remains at rest in the static orbit all time. Particles in such a static orbit, together with particles having zero or small specific angular momentum and specific energy $E^2 \gtrapprox A(r_0)$, can make up a spherical shell consisting of cold gas or fluid. For a distant observer, this shell would look like a shadow similar to that of a black hole.

The expressions for trajectories of timelike and null geodesics can be expressed directly from (12) and (14). They are, respectively,

$$\varphi = J \int \frac{\mathrm{e}^F}{r^2\sqrt{E^2 - V_{\text{eff}}}}\, dr \quad \text{and} \quad \varphi = b \int \frac{\mathrm{e}^F}{r^2\sqrt{1 - b^2A^2/r^2}}\, dr\,.$$

4. Geodesics: analytic examples

For the sake of brevity and simplicity, we will explore a fully analytic, one-parameter family of solutions defined by the functions

$$\xi = \sqrt{r^2 + 2ar + 5a^2} - a, \quad \mathrm{e}^F = \xi' = \frac{r + a}{\sqrt{r^2 + 2ar + 5a^2}}, \tag{15}$$

which uniquely determine the metric function $A(r)$ and the scalar field $\phi(r)$. By direct integration in (6), we obtain

$$A = 1 + \frac{2a}{3r} - 2\,\frac{a + 3m}{15a}\left\{\frac{\sqrt{r^2 + 2ar + 5a^2}}{r}\left(1 + \frac{r}{a} - \frac{r^2}{a^2}\right) + \frac{r^2}{a^2}\right\}, \tag{16}$$

where a is the parameter of 'intensity' of the scalar field. Using (9)–(11) we find that the Kretchmann invariant diverges at the centre. In accordance with the condition $3M < \xi(0)$, the inequality $a > 3/(\sqrt{5} - 1)$ determines the subfamily of scalar field naked singularities.

The results of numerical simulation of geodesics are presented in Figures 1–3.

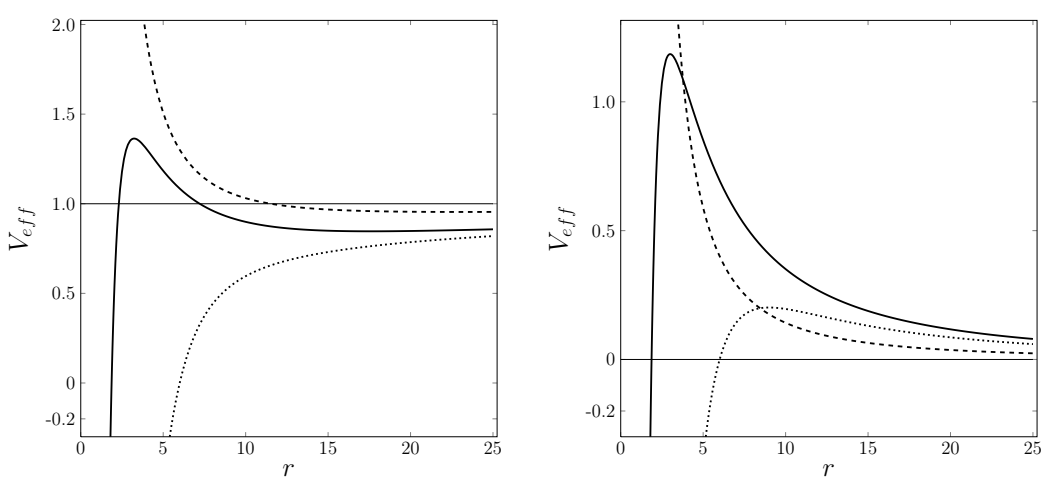

Figure 1. The left (right) panel shows the effective potentials of massive particles (of photons): for the scalar field black hole (solid curve) with $a = 6, M = 3, J = 7.2$ and naked singularity (dashed curve) with $a = 6, M = 1, J = 7.2$, and for the Schwarzschild black hole (dotted curve) with $M = 3, J = 7.2$

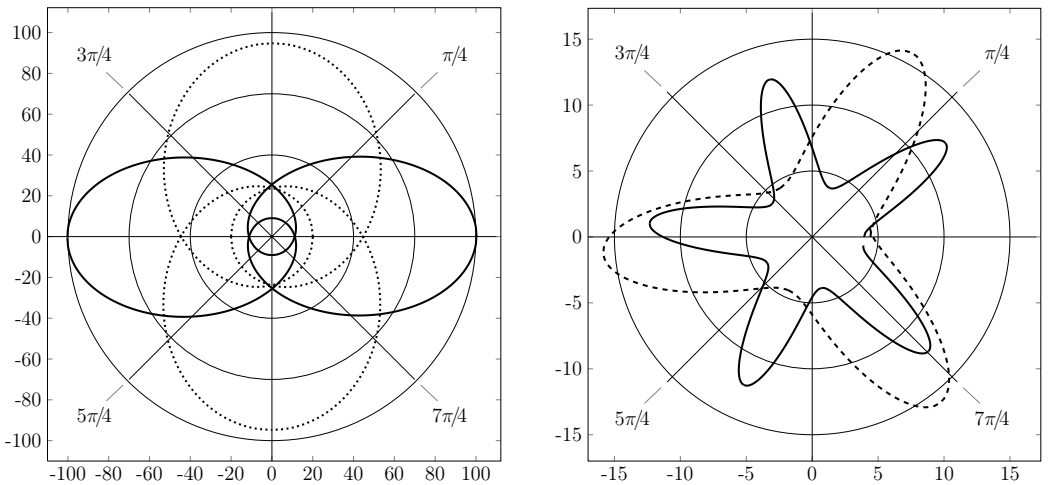

Figure 2. The shape of orbits of massive particles. Left panel: the scalar field black hole with $a = 5, M = 3, J = 9, E^2 = 0.948$ (solid curve) and the Schwarzschild black hole (dotted curve) with $M = 3, J = 12, E^2 = 0.9517$. Right panel: the scalar field naked singularities with $a = 5, M = 1$ and $J = 0.5, , E^2 = 0.88$ (solid curve) and $J = 1, E^2 = 0.9011$ (dashed curve)

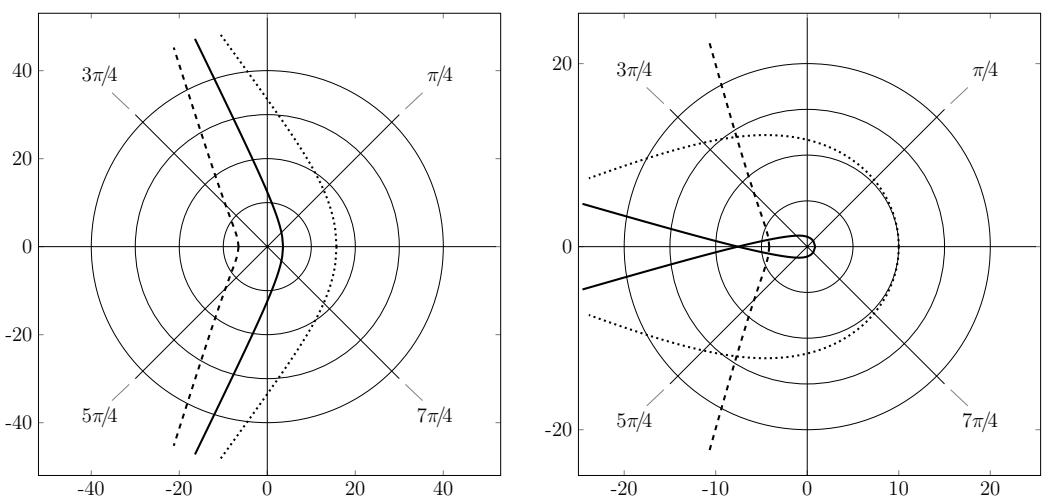

Figure 3. The shape of orbits of photons. Left panel: the scalar field black hole with $a = 7, M = 3, b = 6$ (solid curve), the scalar field naked singularity with $a = 7, M = 1, b = 6$ (dashed curve), and the Schwarzschild black hole (dotted curve) with $M = 3, b = 20$. Right panel: analogously to the left panel, but with parameters $a = 7, M = 3, b = 2.5$ (solid curve), $a = 7, M = 1, b = 2$ (dashed curve), and $M = 3, b = 12$ (dotted curve)

The typical effective potentials are shown in Figure 1, where the difference between timelike and null geodesics is obvious: in particular, the effective potentials of photons in the spacetime of a scalar field naked singularity do

not have extrema, so that there does not exist the photon sphere. In Figure 2, the shape of geodesics for massive test particles are plotted. The shape of an orbit depends on the specific angular momentum J and the specific energy E of a test particle. Numerical simulation shows that the number of oscillations per revolution decreases with increasing J when the value of E is fixed, as well as with decreasing E when the value of J is fixed. Figure 3 presents photon orbits. The difference in the behaviour of null geodesics is obvious.

5. Conclusions

The observations of timelike and null geodesics very close to the centres of galaxies are of great importance, allowing us to study the spacetime geometry near the centres as well as to understand the nature of the central supermassive self-gravitating objects. The available astrophysical data are so far insufficient to identify the strongly gravitating objects and even to definitely distinguish between black holes and naked singularities. However, we can hope that the future development of the spatial resolving power of precise astronomical instruments will be sufficient to observe the central region of Sgr A* (about $15M \approx 0.15mas$). In particular, the facilities of the Event Horizon Telescope are expected to achieve the required sensitivity within the next fifteen years [16], [17].

In this paper, we study (in a fully analytical manner) the characteristic features of the trajectories of null and timelike geodesics in the neighbourhoods of static, spherically symmetric scalar field black holes and naked singularities, having in mind the centre of a galaxy surrounded by dark matter. It turns out that a scalar field black hole, analogously to a Schwarzschild black hole, has the innermost stable circular orbit and the (unstable) photon sphere, but their radii are always less than the corresponding ones for the Schwarzschild black hole of the same mass; moreover, these radii can be arbitrarily small. We show that a scalar field naked singularity has a positive Schwarzschild mass (as opposed to vacuum naked singularities), but has neither the innermost stable circular orbit nor the photon sphere. Instead, such a configuration has a spherical shell of test particles surrounding its origin and remaining in quasistatic equilibrium all the time. We have shown that the characteristic properties of null geodesics near the centres of a scalar field naked singularity and a scalar field black hole of the same mass are qualitatively different. In particular, the quasistatic equilibrium shell can consists of sufficiently cold particles and be observed as a dark shadow surrounded by a photon image. It means that the observation of only the central shadow, circled by a bright ring, is not by itself enough to identify with confidence the central objects. In fact, a key role in the identification of these objects plays observations of the orbits of stars and gas clouds very close to the centre. Note also (this is important for astrophysical applications) that the behaviour of geodesics in the region $r \gtrsim 15m$, where the metrics of a scalar field configuration becomes close to the Schwarzschild one, is qualitatively similar to each other and quantitatively almost the same, so that the observations of the geodesic motion in this region are not sufficiently informative.

References

[1] The EHT collaboration, "First M87 Event Horizon Telescope Results. I. The Shadow of the Supermassive Black Hole," *The Astrophysical Journal Letters*, vol. 875, no. 1, 2019. DOI: 10.3847/2041-8213/ab0ec7.

[2] R. Shaikh, P. Kocherlakota, R. Narayan, and P. S. Joshi, "Shadows of spherically symmetric black holes and naked singularities," *Monthly Notices of the Royal Astronomical Society*, vol. 482, no. 1, pp. 52–64, 2018. DOI: 10.1093/mnras/sty2624.

[3] V. I. Dokuchaev and Y. N. Eroshenko, "Weighing of the dark matter at the center of the Galaxy," *JETP Letters*, vol. 101, no. 12, pp. 777–782, 2015. DOI: 10.1134/S0021364015120048.

[4] A. Hees *et al.*, "Testing General Relativity with stellar orbits around the supermassive black hole in our Galactic center," *Physycal Review Letters*, vol. 118, no. 22, p. 211 101, 2017. DOI: 10.1103/PhysRevLett.118.211101.

[5] A. V. Zakharov, "Constraints on tidal charge of the supermassive black hole at the Galactic Center with trajectories of bright stars," *European Physical Journal C*, vol. 78, p. 689, 2018. DOI: 10.1140/epjc/s10052-018-6166-5.

[6] M. De Laurentis, Z. Younsi, O. Porth, Y. Mizuno, and L. Rezzolla, "Test-particle dynamics in general spherically symmetric black hole spacetimes," *Physical Review D*, vol. 97, no. 10, p. 104 024, 2018. DOI: 10.1103/PhysRevD.97.104024.

[7] G. Z. Babar, A. Z. Babar, and Y. K. Lim, "Periodic orbits around a spherically symmetric naked singularity," *Physical Review D*, vol. 96, no. 8, p. 084 052, 2017. DOI: 10.1103/PhysRevD.96.084052.

[8] I. M. Potashov, J. V. Tchemarina, and A. N. Tsirulev, "Bound orbits near scalar field naked singularities," *European Physical Journal C*, vol. 79, p. 709, 2019. DOI: 10.1140/epjc/s10052-019-7192-7.

[9] K. A. Bronnikov and G. N. Shikin, "Spherically symmetric scalar vacuum: no-go theorems, black holes and solitons," *Gravitation and Cosmology*, vol. 8, pp. 107–116, 2002.

[10] V. V. Nikonov, J. V. Tchemarina, and A. N. Tsirulev, "A two-parameter family of exact asymptotically flat solutions to the Einstein-scalar field equations," *Classical and Quantum Gravity*, vol. 25, no. 13, p. 138 001, 2008. DOI: 10.1088/0264-9381/25/13/138001.

[11] J. V. Tchemarina and A. N. Tsirulev, "Spherically symmetric gravitating scalar fields. The inverse problem and exact solutions," *Gravitation and Cosmology*, vol. 15, pp. 94–95, 2009.

[12] M. Azreg-Ainou, "Selection criteria for two-parameter solutions to scalar-tensor gravity," *General Relativity and Gravitation*, vol. 42, no. 6, pp. 1427–1456, 2010. DOI: 10.1007/s10714-009-0915-6.

[13] D. A. Solovyev and A. N. Tsirulev, "General properties and exact models of static selfgravitating scalar field configurations," *Classical and Quantum Gravity*, vol. 29, no. 5, p. 055 013, 2012. DOI: 10.1088/0264-9381/29/5/055013.

[14] P. V. Kratovitch, I. M. Potashov, J. V. Tchemarina, and A. N. Tsirulev, "Topological geons with self-gravitating phantom scalar field," *Journal of Physics: Conference Series*, vol. 934, no. 1, p. 012 047, Dec. 2017. DOI: 10.1088/1742-6596/934/1/012047.

[15] I. M. Potashov, J. V. Tchemarina, and A. N. Tsirulev, "Bound orbits near black holes with scalar hair," *Journal of Physics: Conference Series*, vol. 1390, no. 1, p. 012 097, Nov. 2019. DOI: 10.1088/1742-6596/1390/1/012097.

[16] S. Gillessen *et al.*, "An update on monitoring stellar orbits in the galactic center," *The Astrophysical Journal*, vol. 837, no. 1, p. 30, 2017. DOI: 10.3847/1538-4357/aa5c41.

[17] C. Goddi *et al.*, "BlackHoleCam: fundamental physics of the Galactic center," *International Journal of Modern Physics D*, vol. 26, no. 2, p. 1 730 001, 2017. DOI: 10.1142/S0218271817300014.

For citation:

I. M. Potashov, J. V. Tchemarina, A. N. Tsirulev, Geodesic motion near self-gravitating scalar field configurations, Discrete and Continuous Models and Applied Computational Science 27 (3) (2019) 231–241. DOI: 10.22363/2658-4670-2019-27-3-231-241.

Information about the authors:

Ivan M. Potashov — Master of Science in Mathematics, Assistant of Department of General Mathematics and Mathematical Physics (e-mail: potashov.im@tversu.ru, ORCID: https://orcid.org/0000-0002-7597-4366, Scopus Author ID: 57200106410)

Julia V. Tchemarina — Candidate of Physical and Mathematical Sciences, Assistant of professor of Department of General Mathematics and Mathematical Physics (e-mail: chemarina.yv@tversu.ru, ORCID: https://orcid.org/0000-0002-9002-887X, Scopus Author ID: 24460923700)

Alexander N. Tsirulev — Doctor of Physical and Mathematical Sciences, Professor of Department of General Mathematics and Mathematical Physics (e-mail: tsirulev.an@tversu.ru, ORCID: https://orcid.org/0000-0003-4168-3613, Scopus Author ID: 16409936300)

УДК 524, 531
PACS 04.20.−q, 04.20.Dw
DOI: 10.22363/2658-4670-2019-27-3-231-241

Геодезическое движение вблизи самогравитирующих конфигураций скалярного поля

И. М. Поташов, Ю. В. Чемарина, А. Н. Цирулев

Математический факультет
Тверской государственный университет
Садовый пер., д. 35, г. Тверь, 170002, Россия

В работе изучается геодезическое движение нейтральных пробных частиц в пространстве-времени статических сферически-симметричных чёрных дыр и голых сингулярностей, порождённых самогравитирующим скалярным полем. Предполагается, что скалярное поле моделирует тёмную материю, окружающую некоторый объект с сильным гравитационным полем, такой как центр нашей Галактики. Поведение времениподобных и изотропных геодезических, проходящих очень близко к центру такой конфигурации, в решающей степени зависит от типа пространства–времени. Оказывается, что скалярно-полевая чёрная дыра, подобно чёрной дыре Шварцшильда, имеет последнюю устойчивую круговую орбиту и (неустойчивую) фотонную сферу, но их радиусы всегда меньше соответствующих радиусов для чёрной дыры Шварцшильда той же массы; кроме того, эти радиусы могут быть сколь угодно малыми. Напротив, голая сингулярность, порождённая скалярным полем, не имеет ни последней устойчивой круговой орбиты, ни фотонной сферы. Вместо этого такая конфигурация имеет сферическую оболочку из частиц, окружающую её центр и всё время находящуюся в квазистатическом равновесии. Также показано, что характерные свойства изотропных геодезических вблизи центра скалярного поля голой сингулярности и центра скалярного поля чёрной дыры, имеющих одинаковую массу качественно различны.

Ключевые слова: геодезическая, чёрная дыра, голая сингулярность, скалярное поле

Computational modeling and simulation

Research article

UDC 517.9
DOI: 10.22363/2658-4670-2019-27-3-242-262

On the properties of numerical solutions of dynamical systems obtained using the midpoint method

Vladimir P. Gerdt[1], **Mikhail D. Malykh**[2], **Leonid A. Sevastianov**[1,2], **Yu Ying**[2,3]

[1] *Joint Institute for Nuclear Research*
Joliot-Curie St. 6, Dubna, Moscow Region 141980, Russian Federation
[2] *Department of Applied Probability and Informatics*
Peoples' Friendship University of Russia (RUDN University)
Miklukho-Maklaya St. 6, Moscow 117198, Russian Federation
[3] *Department of Algebra and Geometry*
Kaili University
Kaiyuan Road 3, Kaili 556011, China

(received: November 20, 2019; accepted: December 23, 2019)

The article considers the midpoint scheme as a finite-difference scheme for a dynamical system of the form $\dot{x} = f(x)$. This scheme is remarkable because according to Cooper's theorem, it preserves all quadratic integrals of motion, moreover, it is the simplest scheme among symplectic Runge-Kutta schemes possessing this property.

The properties of approximate solutions were studied in the framework of numerical experiments with linear and nonlinear oscillators, as well as with a system of several coupled oscillators. It is shown that in addition to the conservation of all integrals of motion, approximate solutions inherit the periodicity of motion. At the same time, attention is paid to the discussion of introducing the concept of periodicity of an approximate solution found by the difference scheme.

In the case of a nonlinear oscillator, each step requires solving a system of nonlinear algebraic equations. The issues of organizing computations using such schemes are discussed. Comparison with other schemes, including those symmetric with respect to permutation of x and $\hat{x}$.

Key words and phrases: conservative finite-difference schemes, dynamical systems, Sage, Maple

Introduction

One of the most common and popular mathematical models is the Cauchy problem for an autonomous system of ordinary differential equations. Analytical methods make it possible to find the algebraic integrals of motion [1] for such systems, and numerical methods allow approximate plotting the particular solutions [2].

Consider an autonomous system of differential equations in an affine space of dimension n

$$\dot{x} = f(x). \tag{1}$$

Here $x = (x_1, \dots, x_n)$ is a point in the affine space, $f = (f_1, \dots, f_n)$ is a set of rational functions belonging to $\mathbb{Q}(x)$. Except the cases where it leads to ambiguity, we will use the vector notation $\dot{x} = f(x)$. By the algebraic integral of motion of this system, we mean the algebraic function g, constant on any particular solution of the system (1), i.e., satisfying the equation

$$f_1 \frac{\partial g}{\partial x_1} + \cdots + f_n \frac{\partial g}{\partial x_n} = 0. \tag{2}$$

It can be shown that the existence of an algebraic integral implies the existence of a rational integral, therefore only rational integrals are considered below [3].

The finite difference method is a standard numerical method for solving systems of ordinary differential equations [2]. The finite-difference scheme for solving the system of equations (1) describes the transition from the value of x taken at some instant of time t to the value of x taken at the next instant of time $t + \Delta t$. This new value will be denoted below by $\hat{x}$. Of course, by the difference scheme for the system (1) we understand a correspondence in some sense approximating the system of differential equations, rather an arbitrary correspondence between the variables x and $\hat{x}$. Usually, by this approximation we mean that the system of equations defining the difference scheme tends to the original system as $\Delta t \to 0$.

Definition 1. By a particular solution of the system (1), found using the finite-difference scheme, we mean a finite or infinite sequence of points

$$x^{(0)}, x^{(1)}, x^{(2)}, \dots, x^{(m)}, \dots$$

of the n-dimensional space (or subset considered in it), the first element of which is taken arbitrarily, and each next element is obtained from the previous one according to the difference scheme:

$$x^{(m+1)} = \hat{x}^{(m)}, \quad m = 0, 1, 2, \dots$$

This approximate particular solution will be associated with the exact solution of the Cauchy problem

$$\dot{x} = f(x), \quad x|_{t=0} = x^{(0)}.$$

Analytical and numerical methods cannot always be reconciled. It often turns out that the algebraic integral of motion is known, but a difference

scheme is used, which does not preserve this integral. Therefore, in numerical experiments, it is often nothing to do but to observe with regret how the quantity which remains constant on the exact solution, changes step by step. Very frequently, the integrals of motion express fundamental laws of nature, the violation of which introduces new properties into the mathematical model under consideration, or trivial geometric relationships, the violation of which makes it difficult to interpret the results of integration.

The idea of contructing finite-difference schemes exactly preserving the integral of motion of dynamical systems was proposed in late 1980s in the papers by Yu. B. Suris [4] and Cooper [5], approaching the problem from different sides, namely, Yu. B. Suris from composing difference schemes for Hamiltonian systems that preserve a symplectic structure, and Cooper from preserving integrals. As a result, a large family of Runge-Kutta schemes was discovered that preserve all quadratic integrals of any dynamical system and the symplectic structure of the Hamiltonian system [6].

The simplest of this class of schemes is the midpoint scheme. By construction, the approximate solutions found using this scheme retain all quadratic integrals. Traditionally, the question of 'improvement' of convergence due to the conservation of integrals remained in the focus of attention. In this article, we intend to clarify what other qualitative properties of the exact solution are inherited by the approximate one. For completeness, we give an elementary proof of Cooper's theorem.

1. Conservation of quadratic integrals

Let g be an integral of the system of Eqs. 1. According to Lagrange theorem about the mean value,

$$g(\hat{x}_1, \dots, \hat{x}_n) - g(x_1, \dots, x_n) = \sum_{i=1}^{n} \frac{\partial g}{\partial x_i}(c_1, \dots c_n) \cdot \Delta x_i,$$

where the derivatives are calculated at the point c, lying somewhere in the segment connecting the points x and $\hat{x}$, i.e., $c_i = x_i + \theta \Delta x_i$, $\theta \in (0, 1)$.

The Lagrange theorem ensures the existence of a suitable function $\theta(x, \hat{x})$, taking the values between 0 and 1 at the real values of $x, \hat{x}$. However, it provides no method to find this function. If we knew such a function, we could easily construct a difference scheme that preserves the manifold $g = 0$ exactly. Indeed, let

$$\frac{\Delta x_i}{\Delta t} = f_i \left(x_i + \theta \Delta x_i \right), \quad i = 1, 2, \dots, n. \tag{3}$$

Then

$$g(\hat{x}_1, \dots, \hat{x}_n) - g(x_1, \dots, x_n) = \sum_{i=1}^{n} \frac{\partial g}{\partial x_i}(c_1, \dots c_n) \cdot f_i(c_1, \dots, c_n),$$

and this expression is exactly equal to zero due to (2).

For some classes of functions, the Lagrange theorem allows a constructive formulation.

Lemma 1. *If g is a polynomial from $\mathbb{C}[x_1, \dots x_n]$, the degree of which does not exceed 2 inclusively, then*

$$g(\hat{x}_1, \dots, \hat{x}_n) - g(x_1, \dots, x_n) = \sum_{i=1}^{n} \frac{\partial g}{\partial x_i}(c_1, \dots c_n) \cdot \Delta x_i,$$

where $c_i = (\hat{x}_i + x_i)/2$.

Proof. Let u be a new auxiliary variable and

$$G(u) = g(x_1 + u\Delta x_1, \dots, x_n + u\Delta x_n).$$

According to the Lagrange theorem, there is such value $\theta \in (0, 1)$, that

$$G(1) - G(0) = G'(\theta), \tag{4}$$

or, in more detail,

$$g(\hat{x}_1, \dots, \hat{x}_n) - g(x_1, \dots, x_n) = \sum_{i=1}^{n} \frac{\partial g}{\partial x_i}(c_1, \dots c_n) \cdot \Delta x_i,$$

where $c_i = x_i + \theta\Delta x_i$.

We have to prove that $\theta = 1/2$.

By the hypothesis of the lemma, g is a polynomial whose degree does not exceed 2, therefore G'' is a polynomial with respect to u whose degree does not exceed 2, i.e.

$$G(u) = au^2 + bu + c, \quad G'(u) = 2au + b.$$

But then the Lagrange formula (4) reduces to $a + b = 2a\theta + b$, from which it immediately follows that $\theta = 1/2$. □

The finite-difference scheme (3) at $\theta = 1/2$, i.e., the scheme

$$\frac{\Delta x_i}{\Delta t} = f_i\left(\frac{\hat{x}_1 + x_1}{2}, \dots, \frac{\hat{x}_n + x_n}{2}\right), \quad i = 1, 2, \dots, n, \tag{5}$$

is called the midpoint scheme. Lemma 1 immediately leads to the following theorem.

Theorem 1 (Cooper, 1983; [5]). *The midpoint finite-difference scheme* (5) *not only approximates the system* (1)*, but also preserves all linear and quadratic integrals of this system.*

2. Harmonic oscillator

Consider the simplest dynamical system

$$\begin{cases} \dot{x} = -y, \\ \dot{y} = x, \end{cases} \tag{6}$$

describing a harmonic oscillator. This system is Hamiltonian, the energy conservation law for it yields the integral $x^2 + y^2 = C$.

Usually it is immediately said without further ado that the solutions of this system describe periodic rotations along concentric circles in the phase plane xy.

The standard discretization does not allow to preserve this description. Consider for definiteness, the explicit Euler scheme

$$\begin{cases} \hat{x} - x = -y\Delta t, \\ \hat{y} - y = x\Delta t. \end{cases}$$

Figure 1 presents the curve in the phase plane, obtained using the Euler method instead of a unit circle. Thus it is easy to describe the difference between the exact and approximate solutions. Instead of closed curves, a spiral in the phase plane appears, or, in terms of classical mechanics, the time discretization leads to gradual increase of the system energy.

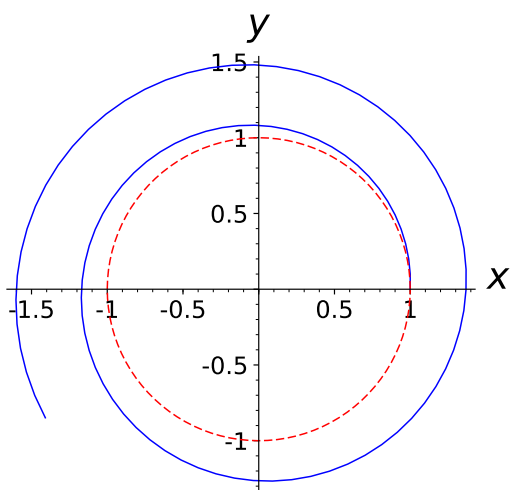

Figure 1. Solution of the initial value problem for Eqs. (6) using the Euler method (solid) and the meanpoint method (dashed), $\Delta t = 0.1$, 100 steps are maid

Now let us consider the meanpoint scheme

$$\hat{x} - x = -(\hat{y} + y)\frac{\Delta t}{2}, \quad \hat{y} - y = (\hat{x} + x)\frac{\Delta t}{2} \tag{7}$$

and try to understand the qualitative difference between the approximate solution and the exact one. According to Cooper's theorem, this difference scheme exaclty preserves this integral. Therefore, in the phase plane we get ovals that seemingly do not differ from a circle (see Figure 1). However, these curves are still not closed, and the motion along them cannot be considered perodic, since the values of x, y do not repeat. Therefore, it could be executed that the absence of closedness and periodicity completely allows one to distinguish between the approximate solution and the exact one. In

fact, it is possible to achieve the solution relativity by the appropriate step choice.

Theorem 2. *If we take for α the minimal positive root of the equation*

$$(1 + i\alpha)^{2N} = (1 + \alpha^2)^N, \tag{8}$$

which in terms of trigonometric functions can be expressed as

$$\alpha = \tan \frac{\pi}{N},$$

then the calculation according to the meanpoint finite-difference scheme (7) *with the step*

$$\Delta t = 2\alpha = 2 \tan \frac{\pi}{N},$$

in N steps leads to the initial values of x, y.

Remark 1. For us it is convenient to use the transcendent formula $\alpha = \tan \frac{\pi}{N}$, however, one could do without it using purely algebraic means. To emphasize this fact, in the statement of the theorem we have preserved the algebraic equation, for which this number is a root.

For proof, let us express $\hat{x}, \hat{y}$ in terms of x, y, denoting for brevity

$$\frac{\Delta t}{2} = \alpha.$$

Then

$$\begin{cases} \hat{x} + \alpha\hat{y} = x - \alpha y, \\ -\alpha\hat{x} + \hat{y} = \alpha x + y \end{cases}$$

or, in the matrix form

$$\begin{pmatrix} 1 & \alpha \\ -\alpha & 1 \end{pmatrix} \begin{pmatrix} \hat{x} \\ \hat{y} \end{pmatrix} = \begin{pmatrix} 1 & -\alpha \\ \alpha & 1 \end{pmatrix} \begin{pmatrix} x \\ y \end{pmatrix}.$$

Inverting the matrix, we get

$$\begin{pmatrix} \hat{x} \\ \hat{y} \end{pmatrix} = \frac{1}{1 + \alpha^2} \begin{pmatrix} 1 & -\alpha \\ \alpha & 1 \end{pmatrix}^2 \begin{pmatrix} x \\ y \end{pmatrix} \tag{9}$$

now the proof of theorem 2 is reduced to the proof of the following purely algebraic lemma.

Lemma 2. *If we take for α the minimal positive root of equation* (8)*, which in terms of trigonometric functions can be written as*

$$\alpha = \tan \frac{\pi}{N},$$

then A^{2N} is a unit matrix.

Proof. Set for brevity

$$A = \frac{1}{\sqrt{1+\alpha^2}} \begin{pmatrix} 1 & -\alpha \\ \alpha & 1 \end{pmatrix}.$$

Assume that we performed N steps of the finite-difference scheme, having started from the values x, y at a certain value $t = 0$, and finished with x^N, y^N at $t = N\Delta t$. Then

$$\begin{pmatrix} x^N \\ y^N \end{pmatrix} = A^2 \begin{pmatrix} x^{N-1} \\ y^{N-1} \end{pmatrix} = \cdots = A^{2N} \begin{pmatrix} x \\ y \end{pmatrix}.$$

The eigenvalues of the matrix A are

$$\lambda_1 = \frac{1+i\alpha}{\sqrt{1+\alpha^2}}, \quad \lambda_2 = \frac{1-i\alpha}{\sqrt{1+\alpha^2}}.$$

When a matrix is raised to a power, its eigenvalues are raised to this power, too.

The equation

$$\lambda_1^{2N} = 1 \tag{10}$$

can be satisfied assuming that

$$\frac{1+i\alpha}{\sqrt{1+\alpha^2}} = \cos\frac{\pi}{N} + i\sin\frac{\pi}{N}$$

or

$$\alpha = \tan\frac{\pi}{N}.$$

The equality (10) can be rewritten in the form of the algebraic equation (8); in this way the minimal positive root of this equation has been found.

At real Δt from the equality (10) the equality $\lambda_2^{2N} = 1$ follows. In this case both eigenvalues of the matrix A^{2N} are equal to 1. The eigenvectors of matrix A are also eigenvectors of any power of this matrix, therefore, in this case two linearly independent eigenvectors correspond to the unit eigenvalue. This is possible only if the matrix A^{2N} coincides with the unit matrix. □

The proved theorem gives rise to the following definition.

Definition 2. The particular solution

$$x, x', x^{(2)}, \ldots$$

found using a certain finite-difference scheme approximating the system (1), at a certain numerical value of the step Δt will be called periodic, if for some $N \in \mathbb{N}$

$$x^{(N)} = x.$$

The number $N\Delta t$ will be called a period of this particular solution.

Theorem 2 means that the midpoint scheme (7) yields periodic solutions at a number of step values that form a descending sequence:

$$\Delta t_3 = 2\tan\frac{\pi}{3} = 2\sqrt{3} = 3.46,$$
$$\Delta t_4 = 2\tan\frac{\pi}{4} = 2,$$
$$\Delta t_5 = 2\tan\frac{\pi}{5} = 2\sqrt{-2\sqrt{5}+5} = 1.45,$$
$$\Delta t_6 = 2\tan\frac{\pi}{6} = \frac{2}{3}\sqrt{3} = 1.15,$$
$$\ldots$$
$$\Delta t_{20} = 2\tan\frac{\pi}{20} = 2\sqrt{5} - 2\sqrt{2\sqrt{5}+5} + 2 = 0.31,$$
$$\ldots$$

converging to zero. The corresponding sequence of periods

$$N\Delta t_N = 2N\tan\frac{\pi}{N} = 2\pi + \frac{2\pi^3}{3}\frac{1}{N^2} + \ldots$$

converges to the exact solution period 2π.

Thus, the second most important qualitative property of the exact solution, i.e., its periodicity, can be preserved, too. Moreover, even for small values of N, in this way it is possible to get a solution that is qualitatively similar to the exact one.

For example, for $N = 10$ and the step value

$$\Delta t = 2\tan\frac{\pi}{10} = \frac{2}{5}\sqrt{-10\sqrt{5}+25} = 0.64$$

we arrive at a periodic scheme with the period $T = 10\Delta t$, that differs from the period of the exact solution by a noticeable value of

$$T - 2\pi = 0.21.$$

In the phase plane xy a regular decagon is obtained that obviously differs from a circle, too. However, even in this case the trajectory in the phase plane is exactly closed and the motion is periodic. In other words, the approximate solution found using the midpoint scheme turns out to be qualitatively similar to the exact one, being rather different quantitatively.

In our opinion, when using the harmonic oscillator model, there is not enough reason to think that the characteristic time scale, taken as physically small, is really small from the point of view of computational mathematics. Therefore, the real reason in favor of using the continuous form of the Newton equations rather than the discrete one is that the traditional method of discretization leads to a violation of the fundamental laws of mechanics (the law of energy conservation) and to a solution, whose properties differ from the expected periodicity. The use of periodic difference schemes removes this difficulty.

3. A system of coupled oscillators

A system of coupled oscillators can be described as a Hamiltonian system with the Hamiltonian

$$H = \sum_{i=1}^{n}\sum_{j=1}^{n} m_{ij}y_iy_j - \sum_{i=1}^{n}\sum_{j=1}^{n} k_{ij}x_ix_j.$$

It is assumed that the kinetic and potential energy

$$\sum_{i=1}^{n} m_{ij}y_iy_j, \quad \sum_{i=1}^{n} k_{ij}x_ix_j$$

are described by positively defined quadratic forms.

In the matrix form the system is written as $M\ddot{\vec{x}} = -K\vec{x}$.

Since the matrices K and M are symmetric and positively defined, the generalized eigenvalue problem $K\vec{\xi} = \lambda M\vec{\xi}$ yields n eigenvectors $\vec{\xi}_1, \dots, \vec{\xi}_n$ that form a basis $\mathbb{R}^n$, orthonormalized with the weight M, corresponding to n positive eigenvalues $\lambda_1 = \omega_1^2, \dots, \lambda_n = \omega_n^2$. In this basis

$$\vec{x} = \sum_{i=1}^{n} z_i(t)\vec{\xi}_i,$$

where $z_i = \vec{\xi}_i^T M\vec{x}$.

The differential equation in these variables is separated into n independent equations

$$\vec{\xi}_j^T M \sum_{i=1}^{n} \ddot{z}_i\vec{\xi}_i = \vec{\xi}_j^T K \sum_{i=1}^{n} z_i\vec{\xi}_i$$

or, due to the basis orthogonality, $\ddot{z}_j + \omega_j^2 z_j = 0$, $j = 1, \dots, n$.

Each of these equations separately describes the vibration of a harmonic oscillator with the frequency ω_j. Therefore, the positive numbers $\omega_1, \dots, \omega_n$ are called eigenfrequencies of the system of coupled oscillators. Now from the formula

$$\vec{x} = \sum_{i=1}^{n} z_i(t)\vec{\xi}_i$$

it is seen that the oscillations of the coupled system will be a superposition of harmonic oscillations at the eigenfrequencies.

Now it is important for us that this system has n algebraic integrals

$$\dot{z}_j^2 + \omega_j^2 z_j^2 = C_j,$$

which in old variables can be written as

$$(\vec{\xi}_i^T M\dot{\vec{x}})^2 + \omega_j^2(\vec{\xi}_i^T M\vec{x})^2 = C_j, \quad j = 1, 2, \dots, n. \tag{11}$$

Thus, the initial system has n quadratic integrals. These integrals will be called partial integrals.

Lemma 3. *If the eigenfrequencies are incommensurable, then any algebraic integral of a system of coupled oscillators is expressed algebraically in terms of n partial integrals.*

The proof of this lemma is somewhat lengthy and is not given here. In essence, it relies on constructions from the proof of Bruns theorem proposed by Painlevé [7].

Remark 2. The condition of incommensurability of frequencies is essential. If $\omega_1 = \omega_2$, then the expression

$$\dot{z}_1 z_2 - z_1 \dot{z}_2 = C$$

is an additional algebraic integral. In fact, the general solution of the system is

$$z_1 = C_1 \cos \omega_1 t + C_2 \sin \omega_1 t, \quad z_2 = C_3 \cos \omega_1 t + C_4 \sin \omega_1 t, ...$$

therefore $\dot{z}_1 z_2 - z_1 \dot{z}_2 = (C_2 C_3 - C_1 C_4)\omega_1$, i.e., is really a constant. Thus, without a separate study, it cannot be ruled out that in degenerate cases the system has additional integrals of motion that are not preserved by the midpoint scheme.

According to the theorem 1, the midpoint scheme preserves all partial integrals, and, therefore, all algebraic integrals of the system.

The step Δt can always be chosen so that the normal oscillation at a certain natural frequency is described by a periodic particular solution. However, this step depends on the harmonic number. Therefore, it is impossible to choose a time step at which the oscillation, in the framework of the continuous model, which is a superposition of periodic normal oscillations (mixed oscillation), would be the sum of periodic particular solutions.

Thus, for the case of linear systems of ordinary differential equations, the midpoint scheme is a difference scheme that preserves all algebraic integrals. Moreover, for periodic particular solutions, it is possible to select a step in a purely algebraic way so that the approximate solution becomes periodic in the sense of the definition 2.

4. Elliptic oscillator

We now proceed to the nonlinear case. Solid state dynamics provides many excellent examples of autonomous systems with periodic solutions. The simplest of them are integrated in Jacobi elliptic functions [8].

By the definition of Jacobi functions [9],

$$p = \operatorname{sn} t, \quad q = \operatorname{cn} t, \quad r = \operatorname{dn} t$$

is a particular solution of the nonlinear autonomous system of differential equations

$$\dot{p} = qr, \, \dot{q} = -pr, \, \dot{r} = -k^2 pq \tag{12}$$

with the initial conditions $p = 0$, $q = r = 1$ at $t = 0$.

This autonomous system has two quadratic integrals of motion

$$p^2 + q^2 = \text{const} \quad \text{and} \quad k^2 p^2 + r^2 = \text{const}. \tag{13}$$

This system is convenient for us, because its properties are not only well studied, but the solutions themselves are easily accessible in any computer algebra system, e.g., in Sage [10].

The system (12) is a convenient test for studying the conservatism of finite-difference schemes used in the common numerical solvers of ordinary differential equations. We, in cooperation with Yu.A. Blinkov, conducted tests on the following systems:

1. lsoda: Real-valued Variable-coefficient Ordinary Differential Equation solver, with fixed-leading-coefficient implementation. It provides automatic method switching between implicit Adams method (for non-stiff problems) and a method based on backward differentiation formulas (BDF) (for stiff problems). Source: `http://www.netlib.org/odepack`;
2. vode: Real-valued Variable-coefficient Ordinary Differential Equation solver, with fixed-leading-coefficient implementation. It provides implicit Adams method (for non-stiff problems) and a method based on backward differentiation formulas (BDF) (for stiff problems). Source: `http://www.netlib.org/ode/vode.f`;
3. dopri5, dop853: This is an explicit Runge-Kutta method of order (4)5 due to Dormand & Prince (with stepsize control and dense output).

In Figures 4–7 it is well seen that in all cases the value of p^2+q^2 increases or decreases almost linearly. Only in the first solver (see Figures 2, 3) "random" fluctuations are observed, but with a trend towards linear growth.

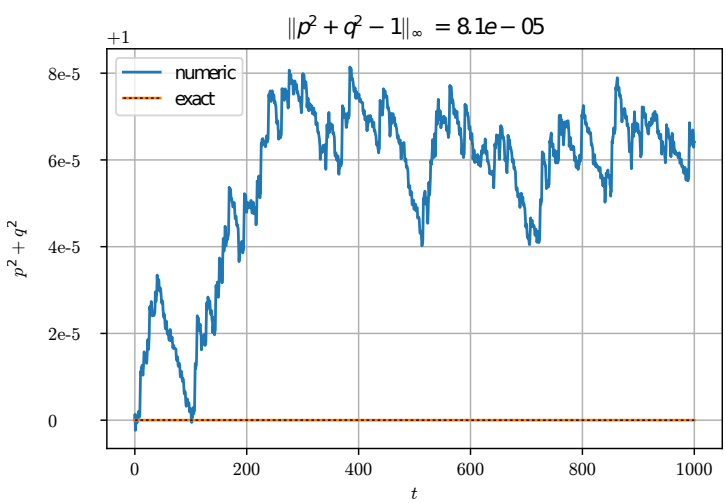

Figure 2. The value of p^2+q^2-1, calculated with the solver Lsoda using the method based on backward differentiation formulas

From an analytical point of view, this system is remarkable because any particular solution of it is representable as the ratio of two everywhere convergent series in powers of t [8]. From the point of view of the finite difference method, this system is remarkable because it can be approximated by a difference scheme, namely, the midpoint scheme (5), which preserves its integrals exactly.

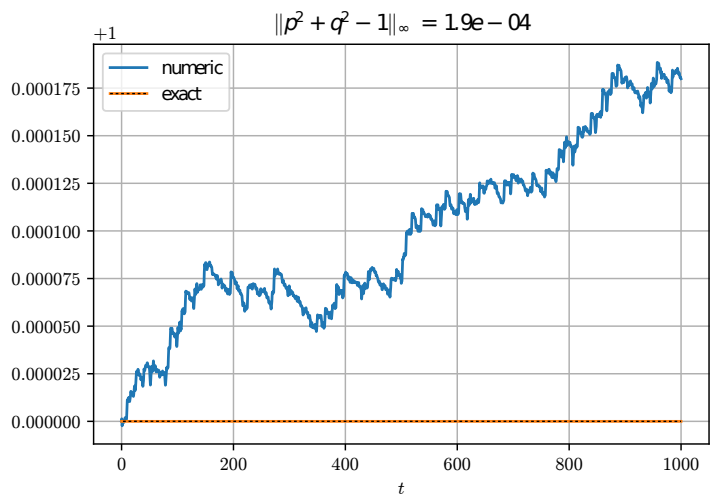

Figure 3. The value of $p^2 + q^2 - 1$, calculated with the solver Lsoda using the method based on the default settings

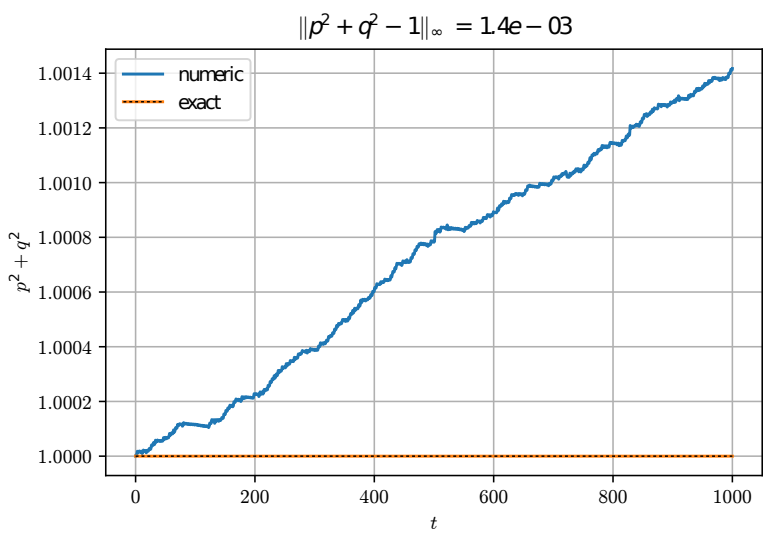

Figure 4. The value of $p^2 + q^2 - 1$, calculated with the solver Vode using the method based on backward differentiation formulas (BDF) with the choice of Jacobian

However, for nonlinear differential equations, the organization of the transition from layer to layer according to the midpoint scheme requires solving a system of nonlinear algebraic equations. The organization of calculations according to such a scheme is a subject of discussion.

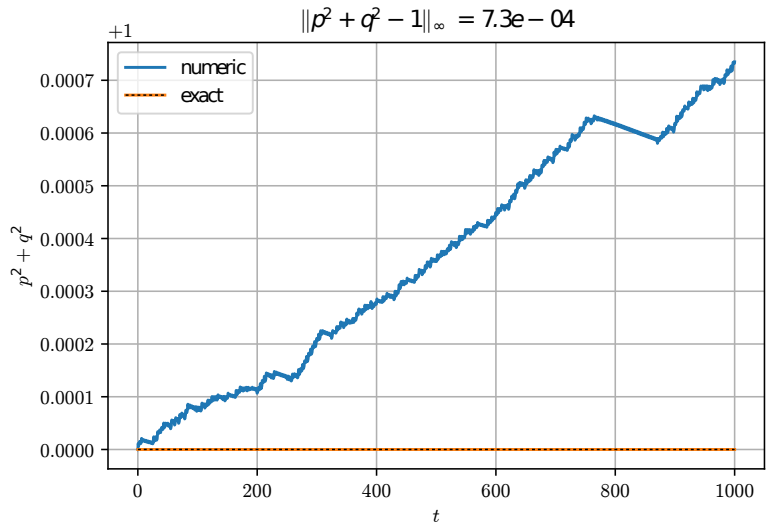

Figure 5. The value of p^2+q^2-1, calculated with the solver Vode using the method based on backward differentiation formulas (BDF) without the choice of Jacobian

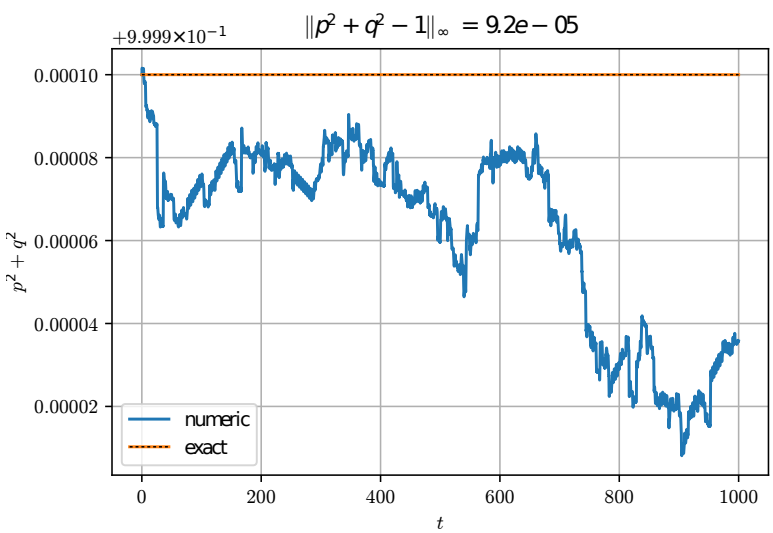

Figure 6. The value of p^2+q^2-1, calculated with the solver Vode using the default settings

The midpoint scheme for the system (12) is written as follows:

$$\begin{cases} \dfrac{\hat{p}-p}{\Delta t} - \dfrac{\hat{q}+q}{2}\dfrac{\hat{r}+r}{2} = 0, \\ \dfrac{\hat{q}-q}{\Delta t} + \dfrac{\hat{p}+p}{2}\dfrac{\hat{r}+r}{2} = 0, \\ \dfrac{\hat{r}-r}{\Delta t} + k^2\dfrac{\hat{p}+p}{2}\dfrac{\hat{q}+q}{2} = 0. \end{cases} \tag{14}$$

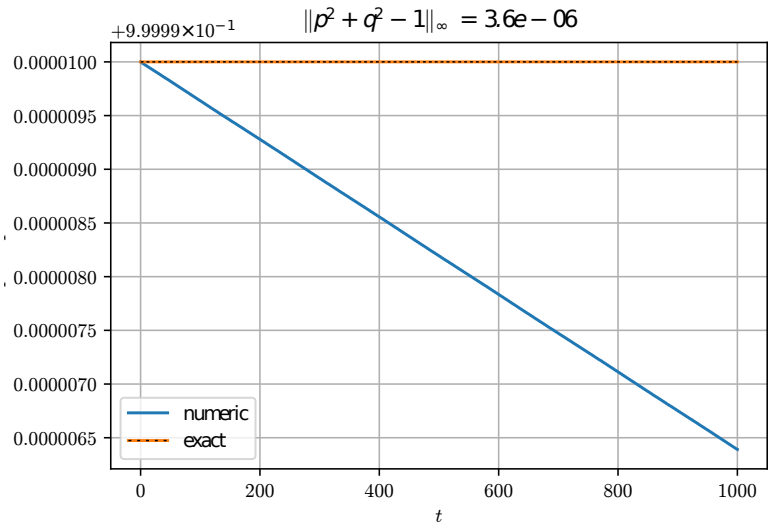

Figure 7. The value of $p^2 + q^2 - 1$, calculated with the solver Dopri5

To pass from one layer to another it is necessary from the given numerical values of Δt and p, q, r to find $\hat{p}$, $\hat{q}$, $\hat{r}$, having solved the system of nonlinear equations. In this case, in addition to the required root, close to the values of p, q, r at small Δt, extraneous roots are also obtained.

Let us investigate this system in Sage, replacing the hat notation with doubling the letter, e.g., using the notation pp instead of $\hat{p}$. The system of equations (14) generates an ideal J in the ring $\mathbb{Q}[p, q, r, \hat{p}, \hat{q}, \hat{r}, \Delta t, k]$.

In Sage this ideal can be specified by the following code:

```
sage: vars=var('p,q,r,pp,qq,rr,dt,k')
sage: K=QQ[vars]
sage: eqs=[4*(pp-p)-(q+qq)*(r+rr)*dt,\
4*(qq-q)+(p+pp)*(r+rr)*dt,\
4*( rr-r)+k^2*(p+pp)*(q+qq)*dt]
sage: J=K.ideal(eqs)
```

Now we can compose an equation connecting $\hat{p}$ with p, q, r by means of elimination ideals [11]:

```
sage: J.elimination_ideal([K(qq),K(rr)]).gens()[0]
```

as

$$p^5\,dt^4k^4 + 3p^4\hat{p}dt^4k^4 + 2p^3\hat{p}^2\,dt^4k^4 - 2p^2\hat{p}^3\,dt^4k^4 - 3p\hat{p}^4\,dt^4k^4 - \hat{p}^5\,dt^4k^4$$
$$+16p^2qr\,dt^3k^2 + 32pqr\hat{p}dt^3k^2 + 16qr\hat{p}^2\,dt^3k^2 - 32p^3\,dt^2k^2 - 64pq^2\,dt^2k^2$$
$$-32p^2\hat{p}dt^2k^2 - 64q^2\hat{p}dt^2k^2 + 32p\hat{p}^2\,dt^2k^2 + 32\hat{p}^3\,dt^2k^2 - 64pr^2\,dt^2 - 64r^2\hat{p}dt^2$$
$$+256qr\,dt + 256p - 256\hat{p} = 0.$$

Thus, one value of p, q, r on the previous layer generally corresponds to 5 different values of $\hat{p}$ rather than one value. Since the higher degrees of $\hat{p}$ enter this equation with the factor Δt, for $\Delta t \to 0$ only one of these roots tends

to a finite value, which is obviously $\hat{p} = p$, and the four others go to infinity. Thus, applying the midpoint scheme to a nonlinear system requires solving a nonlinear equation and then choosing from its roots one root that is 'close' to the values in the previous step.

Traditionally, such equations are solved numerically by iterative methods, and the values of p, q, r are used as the first approximation for $\hat{p}$, $\hat{q}$, $\hat{r}$. If the step Δt is sufficiently small, we can expect the fast convergence of the described method. At the same time, it is not possible to control the error of the iterative method due to the extreme cumbersomeness of the known estimates, and instead the number of iterations is simply fixed. However, as correctly noted in Numerical Recipies [12], there are no universal numerical methods for solving systems of algebraic equations.

Symbolic methods, primarily the Gröbner basis technique, allow us to propose a different approach, circumvent this difficulty, and implement calculations according to the midpoint scheme in a different way:

— the first stage (symbolic analysis of the finite-difference scheme): find equations having the form $P(\hat{p}, p, q, r, \Delta t) = 0$, $Q(\hat{q}, p, q, r, \Delta t) = 0$, $R(\hat{r}, p, q, r, \Delta t) = 0$, that follow from Eq. (14); the first of these equations was written out above;
— the second stage (computations with floating point): to pass from layer to layer solve three uncoupled equations to find $\hat{p}, \hat{q}, \hat{r}$ and select the roots close to the values of p, q, r at the previous layer.

Thus, from the numerical solution of the system of nonlinear equations, we proceed to the solution of one algebraic equation of the 5th degree with numerical coefficients. The methods of numerical solution are well established and in practice give errors close to the errors in calculating a radical from a number.

Remark 3. Unfortunately, the algorithms implemented in Sage do not give us, together with the roots, an estimate of this error. The question of the precision solution of algebraic equations with real coefficients is currently discussed at all conferences on numerical methods and computer algebra (MMA'2018, CASC'2019). We hope that in the near future this issue will be completely closed.

We implemented both approaches to the implementation of the midpoint method and made sure that the first approach gives the same result faster. Figures 8–9 show the elliptic sine plot calculated in Sage using the built-in algorithm for calculating elliptic functions and directly using the midpoint method. It is clearly seen that even at extremely large values of t, the oscillation amplitude does not decrease. Thus, when using the midpoint scheme:

— both algebraic integrals of motion are preserved exactly,
— rounding error does not accumulate in a way that is noticeable in numerical experiments,
— the periodic nature of the motion is preserved.

A theoretical study of the last two issues faces significant difficulties, which, in our opinion, make us search not for any conservative schemes, but for schemes in which the transition from layer to layer requires solving linear equations. One such scheme for the elliptic oscillator (12) was specified by us

in [13]; in the general case of the system (1) there are fundamental obstacles to the existence of such schemes [14].

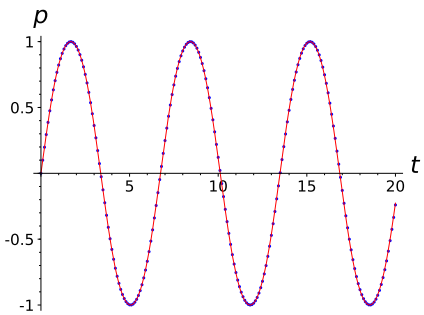

Figure 8. $\mathrm{sn}\left(t, \frac{1}{2}\right)$, $N = 200$

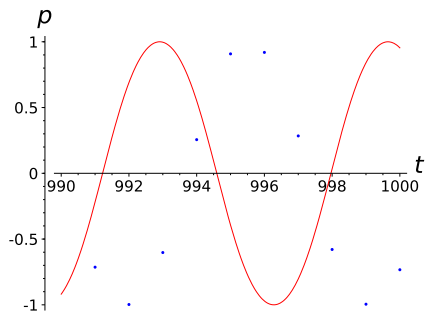

Figure 9. $\mathrm{sn}\left(t, \frac{1}{2}\right)$, $N = 200$

5. Comparing midpoint scheme with other symmetric schemes

One could think that the conservation of integrals is the result of the scheme symmetry. Therefore, for completeness, we compare the midpoint scheme with another popular symmetric second-order scheme:

$$\frac{\Delta x}{\Delta t} = \frac{f(\hat{x}) + f(x)}{2}. \tag{15}$$

The results of our numerical experiments, presented in the Figure 10, show that this scheme does not preserve the integrals, but gives them values that oscillate with a constant period around some fixed value. This can be accepted for preserving the integrals of the motion on average.

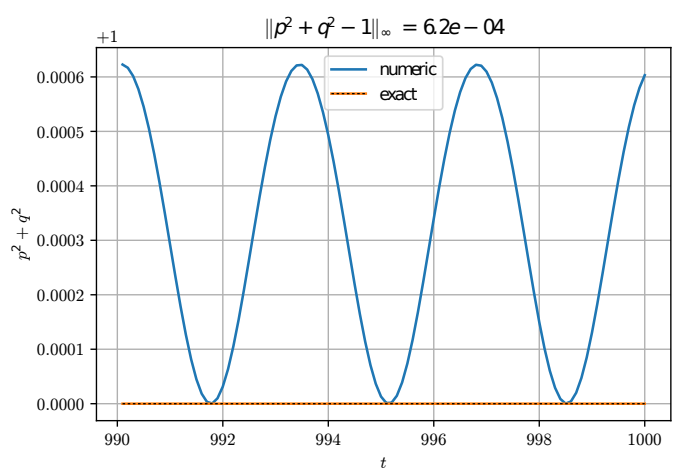

Figure 10. The value of $p^2 + q^2 - 1$, calculated using the scheme (15)

This effect can be explained as follows. The scheme (15) for the Jacobi system yields

$$\Delta p = \frac{\hat{q}\hat{r} + qr}{2}\Delta t, \quad \Delta q = -\frac{\hat{p}\hat{r} + pr}{2}\Delta t, \quad \Delta r = -k^2\frac{\hat{p}\hat{q} + pq}{2}\Delta t. \tag{16}$$

Therefore

$$\begin{aligned}\Delta(p^2+q^2) = (\hat{p}+p)\Delta p + (\hat{q}+q)\Delta q = \\ = [(\hat{p}+p)(\hat{q}\hat{r}+qr) - (\hat{q}+q)(\hat{p}\hat{r}+pr)]\frac{\Delta t}{2} = \\ = [p\hat{q}\hat{r} + \hat{p}qr - \hat{q}pr - q\hat{p}\hat{r}]\frac{\Delta t}{2} = \\ = (p\hat{q} - \hat{p}q)\Delta r\frac{\Delta t}{2} = (p\Delta q - q\Delta p)\Delta r\frac{\Delta t}{2} = \\ = -[p(\hat{p}\hat{r}+pr) + q(\hat{q}\hat{r}+qr)]\Delta r\frac{\Delta t^2}{4} = \\ = [(p\hat{p}+q\hat{q})\hat{r} + (p^2+q^2)r](\hat{p}\hat{q}+pq)\frac{k^2\Delta t^3}{8}\end{aligned} \tag{17}$$

or, expanding in series in powers of Δt

$$\Delta(p^2+q^2) = (p^2+q^2)pqr\frac{k^2\Delta t^3}{2} + \dots .$$

For small Δt in the plot of p^2+q^2 versus the step number (or, which is similar, versus t) we will see periodic oscillations of the first term

$$(p^2+q^2)pqr\frac{k^2\Delta t^3}{2}.$$

Thus, the oscillation of the value of the integral p^2+q^2 near its exact value 1 observed in the numerical experiment is not related to the conservativeness of the scheme, but is due to the fact that the main term in the expansion of the increment of this integral in power of t depends on the values of p, q, r, approximating periodic functions. The considered representation scheme is a perfect example of the scheme symmetric with respect to permutation of x and $\hat{x}$.

Conclusion

For the study of dynamical systems with quadratic integrals, the midpoint scheme is perfect. This scheme preserves all the integrals of these systems precisely, that is, discretization does not introduce any dissipativity or antidissipativity into the model.

Linear problems have just quadratic integrals, and the calculation according to the midpoint scheme requires solving linear equations, so the issue of constructing conservative difference schemes for linear differential equations

can be considered closed. It worth noting that the Kepler problem after passing to proper time and introducing the Runge-Lenz-Laplace vector turns into a linear dynamical system, therefore, it is possible to construct for it a conservative finite-difference scheme [15].

Conservation of integrals leads to the preservation of a number of qualitative properties of the model, e.g., the periodicity of solutions and the closedness of phase trajectories.

The calculation according to the midpoint scheme for nonlinear systems, even if all their integrals are quadratic, makes it necessary to solve a nonlinear system of algebraic equations at each step, which significantly complicates both the calculation and the study of the properties of approximate solutions. Overcoming this difficulty is the main challenge of the theory of difference schemes for ordinary differential equations.

Acknowledgments

The studies of difference schemes that inherit the properties of a continuous model carried out by V. P. Gerdt and L. A. Sevastianov were supported by the RUDN 5–100 program. The calculation results presented in Figures 2–7 and 10 were obtained by V. P. Gerdt together with Yu. A. Blinkov in the SymPy system and were first presented at the PCA'2019 conference [16]. The authors are grateful to Yu. A. Blinkov for the materials provided. Calculations using the midpoint scheme were performed in the Sage system by M. D. Malykh and Yu Ying as part of studies supported by RFBR grant No. 18-51-18005.

References

[1] A. Goriely, *Integrability and nonintegrability of dynamical systems*. Singapore; River Edge, NJ: World Scientific, 2001.

[2] E. Hairer, G. Wanner, and C. Lubich, *Geometric numerical integration. Structure-preserving algorithms for ordinary differential equations*. Berlin Heidelberg New York: Springer, 2000.

[3] L. Königsberger, *Die Principien der Mechanik*. Leipzig: Teubner, 1901.

[4] Y. B. Suris, "Hamiltonian methods of Runge–Kutta type and their variational interpretation [Gamil'tonovy metody tipa Runge–Kutty i ikh variatsionnaya traktovka]," *Matematicheskoye modelirovaniye*, vol. 2, no. 4, pp. 78–87, 1990, in Russian.

[5] G. J. Cooper, "Stability of Runge–Kutta methods for trajectory problems," *IMA Journal of Numerical Analysis*, vol. 7, pp. 1–13, 1987. DOI: 10.1093/imanum/7.1.1.

[6] J. M. Sanz-Serna, "Symplectic Runge–Kutta schemes for adjoint equations, automatic differentiation, optimal control, and more," *SIAM REVIEW*, vol. 58, pp. 3–33, 1 2016. DOI: 10.1137/151002769.

[7] P. Painlevé, "Mémore sur les intégrales du problème des n corps," in *Œuvres de Paul Painlevé*. 1975.

[8] V. V. Golubev, *Vorlesungen über Differentialgleichungen im Komplexen*. Leipzig: VEB Deutscher Verlag der Wissenschaften, 1958.

[9] P. F. Byrd and M. D. Friedman, *Handbook of elliptic integrals for engineers and scientists*. Springer, 1971. DOI: 10.1007/978-3-642-65138-0.

[10] W. A. Stein. (2015). Sage Mathematics Software (Version 6.7), The Sage Development Team, [Online]. Available: http://www.sagemath.org.

[11] D. A. Cox, J. Little, and D. O'Shea, *Ideals, varieties, and algorithms: an introduction to computational algebraic geometry and commutative algebra*, 4th ed. Springer, 2015. DOI: 10.1007/978-3-319-16721-3.

[12] *Numerical Recipes: The Art of Scientific Computing*, 3rd ed. Cambridge University Press, 2007, 1256 pp.

[13] E. A. Ayryan, M. D. Malykh, L. A. Sevastianov, and Yu Ying, "Finite difference schemes and classical transcendental functions," *LNCS*, vol. 11189, pp. 3–33, 2019. DOI: 10.1007/978-3-030-10692-8_26.

[14] E. A. Ayryan, M. D. Malykh, L. A. Sevastianov, and Yu Ying, "On explicit difference schemes for autonomous systems of differential equations on manifolds," *LNCS*, vol. 11661, pp. 343–361, 2019. DOI: 10.1007/978-3-030-26831-2_23.

[15] R. Kozlov, "Conservative discretizations of the Kepler motion," *Journal of Physics A*, vol. 40, no. 17, pp. 4529–4539, 2007. DOI: 10.1088/1751-8113/40/17/009.

[16] Y. A. Blinkov and V. P. Gerdt, "On computer algebra aided numerical solution of ODE by finite difference method," in *Polynomial Computer Algebra '2019. April 15–20, 2019. Euler International Mathematical Institute, St. Petersburg, RUSSIA*. 2019.

For citation:

V. P. Gerdt, M. D. Malykh, L. A. Sevastianov, Yu. Ying, On the properties of numerical solutions of dynamical systems obtained using the midpoint method, Discrete and Continuous Models and Applied Computational Science 27 (3) (2019) 242–262. DOI: 10.22363/2658-4670-2019-27-3-242-262.

Information about the authors:

Vladimir P. Gerdt — Doctor of Physical and Mathematical Sciences, Full Professor at the Joint Institute for Nuclear Research (JINR) where he is the head of the Group of Algebraic and Quantum Computations (e-mail: gerdt@jinr.ru, phone: + 7 (49621) 63437, ORCID: https://orcid.org/0000-0002-0825-1811, ResearcherID: T-5179-2019, Scopus Author ID: 57209076002)

Mikhail D. Malykh (Russian Federation) — Candidate of Physical and Mathematical Sciences, assistant professor of Department of Applied Probability and Informatics of Peoples' Friendship University of Russia (RUDN University) (e-mail: malykh-md@rudn.ru, phone: +7(495)9550927, ORCID: https://orcid.org/0000-0001-6541-6603, ResearcherID: P-8123-2016, Scopus Author ID: 6602318510)

Yu Ying (China) — postgraduate student of Department of Applied Probability and Informatics of Peoples' Friendship University of Russia (RUDN University); assistant professor of Department of Algebra and Geometry, Kaili University (e-mail: yingy6165@gmail.com, phone: +7(495)9550927, ORCID: https://orcid.org/0000-0002-4105-2566, ResearcherID: AAC-8344-2019, Scopus Author ID: 57208127921)

Leonid A. Sevastianov (Russian Federation) — professor, Doctor of Physical and Mathematical Sciences, professor of Department of Applied Probability and Informatics of Peoples' Friendship University of Russia (RUDN University) (e-mail: sevastianov-la@rudn.ru, phone: +7(495)955-07-83, ORCID: https://orcid.org/0000-0002-1856-4643, ResearcherID: B-8497-2016, Scopus Author ID: 8783969400)

УДК 517.9
DOI: 10.22363/2658-4670-2019-27-3-242-262

О свойствах численных решений динамических систем, полученных по схеме средней точки

В. П. Гердт[1], **М. Д. Малых**[2], **Л. А. Севастьянов**[1,2], **Юй Ин**[2,3]

[1] *Объединенный институт ядерных исследований*
ул. Жолио Кюри, д. 6, г. Дубна, Московская область, 141980, Россия
[2] *Кафедра прикладной информатики и теории вероятностей*
Российский университет дружбы народов
ул. Миклухо-Маклая, д. 6, г. Москва, 117198, Россия
[3] *Кафедра алгебры и геометрии*
Университет Каили
Kaiyuan Road 3, Каили 556011, Китай

В статье рассматривается схема средней точки как разностная схема для динамической системы вида $\dot{x} = f(x)$. Эта схема замечательна тем, что в силу теоремы Купера сохраняет все квадратичные интегралы движения, более того, это — простейшая схема из числа симплектических схем Рунге–Кутты, обладающих названным свойством.

Свойства приближённых решений изучены в рамках численных экспериментов с линейным и нелинейным осцилляторами, а также с системой нескольких связанных осцилляторов. Показано, что помимо сохранения всех интегралов движения, приближённые решения наследуют периодичность движения. При этом уделено внимание обсуждению введения понятие периодичности приближённого решения, найденного по разностной схеме.

В случае нелинейного осциллятора выполнение каждого шага требует решения системы нелинейных алгебраических уравнений. Обсуждены вопросы организации вычислений по таким схемам. Дано сравнение с другими схемами, в том числе симметрическими относительно перестановки x и $\widehat{x}$.

Ключевые слова: консервативные конечно-разностные схемы, динамические системы, Sage, Maple

Methodological article

PACS 07.05.Tp, 02.70.-c, 02.60.Cb
DOI: 10.22363/2658-4670-2019-27-3-263-267

Computational experiment in era of HPC

Alexander S. Ayriyan[1,2]

[1] *Laboratory of Information Technologies*
Joint Institute for Nuclear Research
6 Joliot-Curie St., Dubna, Moscow Region 141980, Russian Federation
[2] *Computational Physics and IT Division*
A. I. Alikhanyan National Science Laboratory, Yerevan, Armenia

(received: December 19, 2019; accepted: December 23, 2019)

In this note we discuss the impact of development of architecture and technology of parallel computing on the typical life-cycle of the computational experiment. In particular, it is argued that development and installation of high-performance computing systems is indeed important itself regardless of specific scientific tasks, since the presence of cutting-age HPC systems within an academic infrastructure gives wide possibilities and stimulates new researches.

Key words and phrases: computational experiment, high performance computing systems, Mathematical modelling

1. Introduction

The scheme of a computational experiment is the procedure for carrying out research of physical phenomena and technical devices based on the triad of mathematical modeling: `model` → `algorithm` → `program` [1], [2]. More often, the study is conducted for granted; in this sense, the scheme of a computational experiment is retrospective. However, to some extent, it is useful to consider such a scheme in detail for both creating an overall picture of research *a posteriori* and planning it *a priori*.

2. Stages of computational experiment

A computational experiment is based on *a priori* knowledge of the object under study, namely, theoretical and empirical data, established and generally accepted phenomenological models. Each cycle of a computational experiment consists of the following stages:

1. Building a model of the considered phenomenon under study (making up equations describing the phenomenon).

2. Formulation of a mathematical problem (formulating initial, boundary value, initial boundary value problems, optimization problems, etc.).
3. Choosing numerical methods for solving the problem (building difference schemes, choosing and/or developing algorithms, parallelization of calculations, etc.).
4. Realization of a program that implements the algorithms.
5. Choosing a suitable computing architecture, compiling and running programs on a computing system (selecting a compiler, collecting libraries of necessary algorithms).
6. Carrying out calculations and processing the obtained data (bringing the output data to the form necessary for their further analysis).
7. Analyzing the results; if possible, comparing them with a full-scale experiment.

3. Description of the stages

Quite often, at the last stage one starts to understand what changes should be made to the previous stages. At the same time, the cycle of a computational experiment begins once again, with the first stage, when some changes should be made to the model of the considered phenomenon, if the built model does not reflect well enough the peculiarities of the phenomenon or it becomes necessary to make changes to the model parameters.

The cycle can be repeated in a shorter form, for example, from the second stage, if any changes need to be made to the mathematical formulation of the problem. It may turn out that the used numerical methods have some drawbacks in terms of accuracy, efficiency or applicability; in this case, one will have to start the cycle of a computational experiment from the third stage.

The cycle of a computational experiment will begin with the fourth stage if the software implementation turns out to be ineffective in terms of calculation speed, code readability, its extensibility and scalability; in this case, one will have to make changes to the existing code or choose another programming environment.

Due to the unsatisfactory time of calculations, one may need to choose another computing environment that has more RAM, a better data transfer interface (in case of parallel computing), a more suitable file system, a better architecture and/or a set of compilers, which, in turn, can significantly reduce the estimated time and increase the efficiency of the cycle of a computational experiment. In this case, the cycle starts from the fifth stage, as there is no need to make changes to stages 1 to 4.

The exit from the cycle of a computational experiment happens when, after analyzing the results, the study is considered complete.

In the literature the fifth stage is not included in the description of a computational experiment ("Computational system" in Figure 1) (see, for example, [2], [3]), however, due to the development of novel computing architectures showing high efficiency in solving certain classes of problems, and to the increase of their availability, it becomes necessary to explicitly include this stage in the cycle of a computational experiment. When a researcher has access to

hybrid computational systems, such as HybriLIT [4], [5] containing different computing architectures, it gives him wide potential for the study.

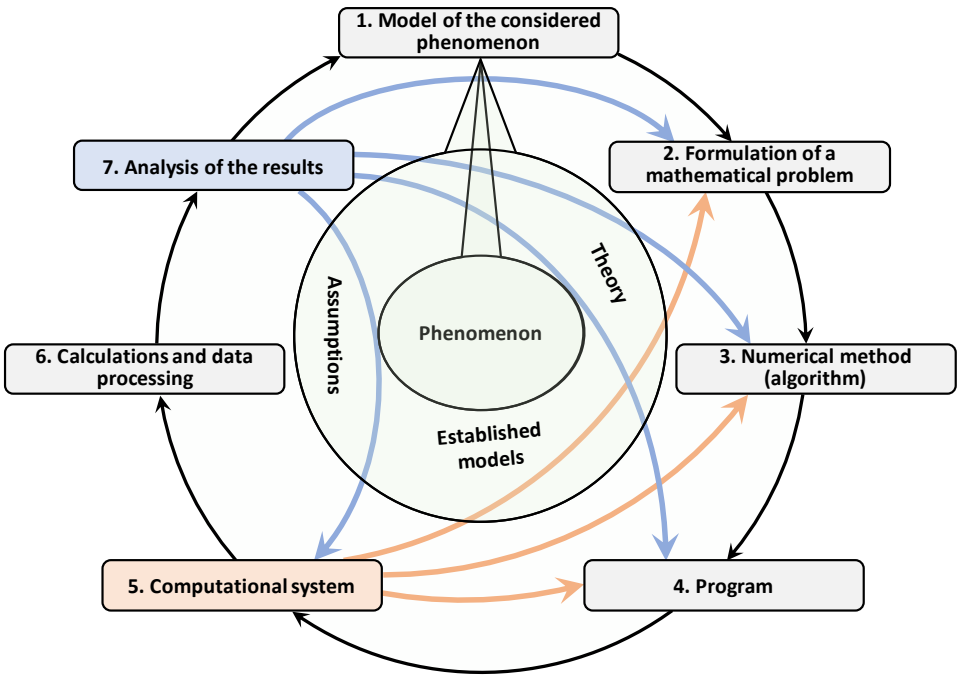

Figure 1. The scheme of a computational experiment

In this case, it becomes possible to reformulate the mathematical problem to another, which will require large computational costs, but will be more suitable for carrying out research, for example, to replace the initial boundary value problem with an optimization problem if the model is parameterized and it is possible to formulate an optimization criterion (see, for example, [6]).

The choice of a computational method becomes wider; one can choose a method that is easier to implement, but more effective with a larger amount of computing resources. One of the great illustrations is the direct enumeration (or search) method; if there are sufficient computing resources, such a method can be extremely effective in terms of the calculation time. Finally, the characteristics of a computing system can directly influence the software implementation of computational methods.

4. Conclusion and discussion

Thus, one may conclude that the efficiency of a computational experiment directly depends on the available computing ecosystem. From this it follows that an HPC ecosystem must be developed regardless of the demands and tasks, since it itself affects the development of scientific studies.

References

[1] "Mathematical modeling and computational experiment [Matematicheskoye modelirovaniye i vychislitel'nyy eksperiment]," *Bulletin of USSR Academy of Science [Vestnik AN SSSR]*, vol. 49, no. 5, A. A. Samarsky, Ed., pp. 38–49, 1979, in Russian.

[2] "Computational experiment in technology problems [Vychislitel'nyy eksperiment v zadachakh tekhnologii]," *Bulletin of USSR Academy of Science [Vestnik AN SSSR]*, vol. 54, no. 3, A. A. Samarsky, Ed., pp. 77–88, 1984, in Russian.

[3] M. M. Gorbunov-Posadov, *Extensible programs [Rasshiryayemyye programmy]*. Moscow: Polyptych, 1999, in Russian.

[4] HybriLIT group. (2019). Heterogeneous platform "HybriLIT", [Online]. Available: `http://hlit.jinr.ru/en/`.

[5] G. Adam *et al.*, "IT-ecosystem of the HybriLIT heterogeneous platform for high-performance computing and training of IT-specialists," English, in *CEUR Workshop Proceedings*, V. Korenkov, A. Nechaevskiy, T. Zaikina, and E. Mazhitova, Eds., vol. 2267, 2018, pp. 638–644.

[6] A. Ayriyan, J. Buša Jr., H. Grigorian, and E. E. Donets, "Solving the optimization problem for designing a pulsed cryogenic cell," *Physics of Particles and Nuclei Letters*, vol. 16, no. 5, pp. 300–309, 2019. DOI: `10.1134/S1547477119030026`.

For citation:

A. S. Ayriyan, Computational experiment in era of HPC, Discrete and Continuous Models and Applied Computational Science 27 (3) (2019) 263–267. DOI: 10.22363/2658-4670-2019-27-3-263-267.

Information about the authors:

Alexander S. Ayriyan (Russian Federation) — Researcher of the Laboratory of Information Technologies, Joint Institute for Nuclear Research (Dubna, Russia), and Computational Physics and IT Division, A. I. Alikhanyan National Science Laboratory (Yerevan, Armenia) (e-mail: `ayriyan@jinr.ru`, ORCID: https://orcid.org/0000-0002-5464-4392, ResearcherID: O-5259-2015, Scopus Author ID: 24528624400)

PACS 07.05.Tp, 02.70.-c, 02.60.Cb
DOI: 10.22363/2658-4670-2019-27-3-263-267

Вычислительный эксперимент в эпоху HPC

А. С. Айриян[1,2]

[1] *Научный отдел вычислительной физики*
Лаборатория информационных технологий
Объединённый институт ядерных исследований
ул. Жолио Кюри, д. 6, г. Дубна, Московская область, 141980, Россия
[2] *Научный отдел вычислительной физики и ИТ*
Национальная научная лаборатория им. А. Алиханяна, Ереван, Армения

В данной заметке обсуждается влияние развития архитектуры и технологии параллельных вычислений на цикл вычислительного эксперимента. В частности, делается вывод, что разработка и установка высокопроизводительных вычислительных систем действительно важна сама по себе, вне зависимости от конкретных научных задач, поскольку наличие современных высокопроизводительных вычислительных систем в академической инфраструктуры даёт широкие возможности и стимулирует новые исследования.

Ключевые слова: вычислительный эксперимент, высокопроизводительные вычислительные системы, математическое моделирование